Available online at www.sciencedirect.com
SCIENCE DIRECT
Icarus 172 (2004) 582–602
ICARUS
www.elsevier.com/locate/icarus

Strike-slip fault evolution on Europa: evidence from tailcrack geometries

Simon A. Kattenhorn *

Department of Geological Sciences, University of Idaho, PO Box 443022, Moscow, ID 83844-3022, USA

Received 30 April 2004; revised 12 July 2004

Available online 15 September 2004

Abstract

Secondary cracks are commonly produced at stress concentration points at the tips of slipping interfaces such as faults. These so-called tailcracks form an antisymmetric pattern at opposite tips of the fault with a fracture geometry that is a mechanical indicator of the sense of slip, whether left-lateral or right-lateral. I present descriptions of tailcracks along numerous strike-slip faults on Europa. Two distinct styles of strike-slip faults are identified: ridge-like and band-like. The angles between faults and tailcracks are variable and are commonly less than the theoretical 70.5° angle that approximately characterizes many terrestrial examples involving fault surfaces that remain in contact during slip. Median tailcrack angles are lower for band-like faults (30°) than ridge-like faults (52°). In addition, the sense of curvature of band-like fault tailcracks is characteristically opposite to that of ridge-like faults. Analytical models of stress orientations around strike-slip faults on Europa indicate that these effects result from dilation during strike-slip motion. Band-like faults characteristically underwent concurrent dilation and shearing but this dynamic coupling is not characteristic of ridge-like faults. The implication is that strike-slip faulting was not a globally homogeneous process on Europa and as a result the morphologies of strike-slip faults are variable. Furthermore, band-like faults appear to corroborate the predictions of the tidal walking theory, exhibiting predominantly right-lateral motions in the southern hemisphere and left-lateral motions in the northern hemisphere. However, ridge-like faults do not obey this slip-sense convention, suggesting that the tidal walking theory may be appropriate for describing the evolution of dilational band-like faults but that ridge-like faults may have resulted from a different driving mechanism.

Keywords: Europa; Tectonics; Surfaces, satellite

1. Introduction

Jupiter's moon, Europa, has a pervasively fractured ice shell that is generally believed to overlie an inviscid ocean having a combined thickness in the 100–170 km range (Anderson et al., 1998; Carr et al., 1998; Pappalardo et al., 1999; McKinnon, 2004). Imaging of Europa's surface by the Voyager and Galileo spacecraft indicated that the fractures (or lineae) occur over a range of scales, with lengths from hundreds of meters (the smallest dimensions discernible in the highest resolution images) to over two thousand kilometers. These lineae exhibit a variety of morphologies (Geissler et al., 1998; Prockter et al., 1999; Figueredo and Greeley, 2000, 2004; Greeley et al., 2000; Kattenhorn, 2002), ostensibly in response to disparate formation mechanisms or due to different stages in an evolutionary sequence of fracture development. For example, there is an apparent morphologic continuum of fracture types from troughs (surface fractures) to ridges to bands (Geissler et al., 1998; Greenberg et al., 1998; Pappalardo et al., 1998), implying that these features progressively develop over perhaps millions of years as they are repeatedly reworked by stresses in the ice shell. The greatest number of lineae appear to be ridges, which formed throughout the visible geologic history (Kattenhorn, 2002), creating a complex sequence of cross-cutting fractures. Piercing points to either side of these ridges typically show zero lateral offsets, suggesting that the ridges either formed as two walls of a fracture simply pulled apart from each other with the opening vector oriented perpendicular to the fracture trend, or that any potential shear

* Fax: (208)885-5724.
E-mail address: simkat@uidaho.edu.

0019-1035/$ – see front matter
doi:10.1016/j.icarus.2004.07.005

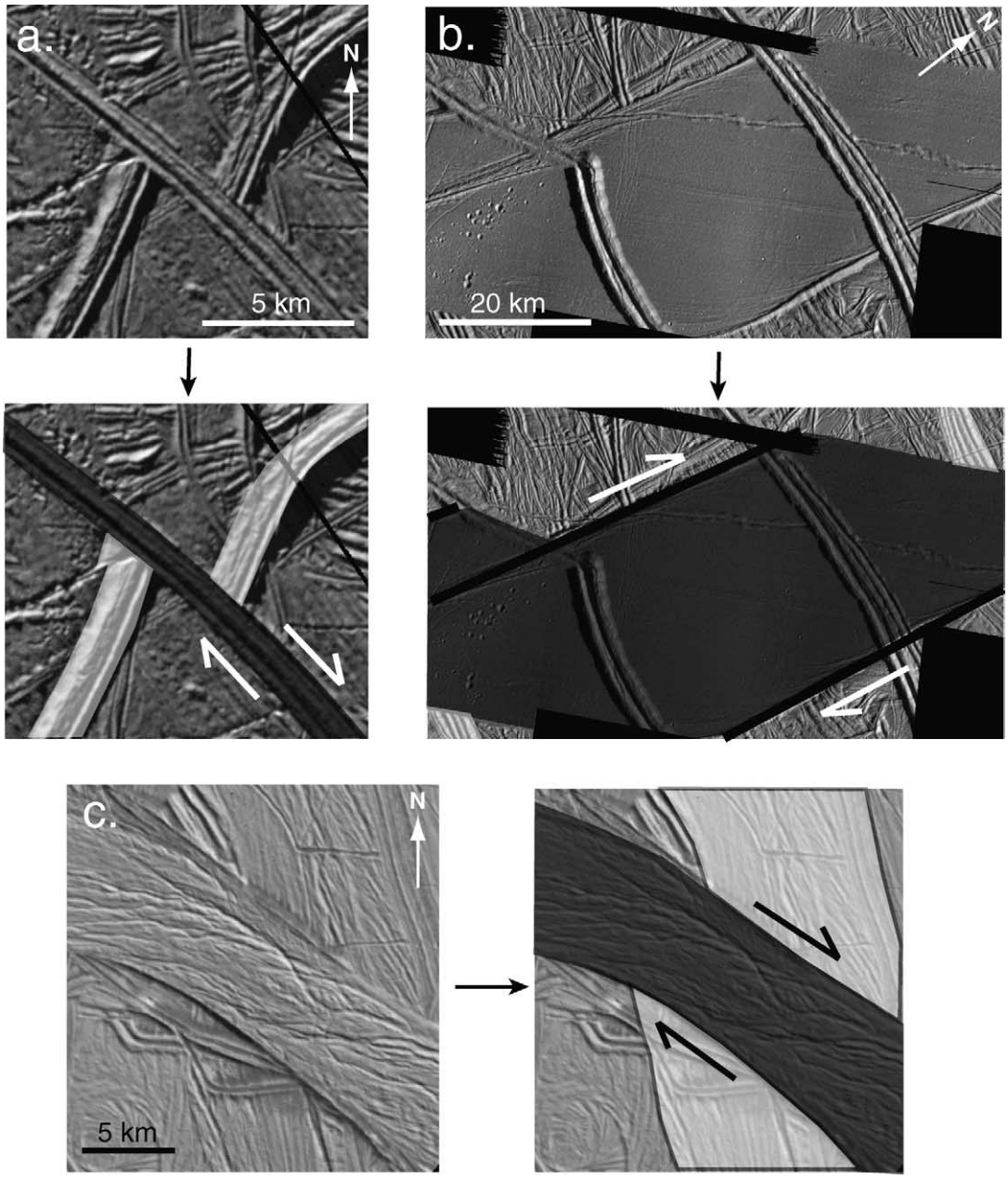

Fig. 1. Examples of different styles of strike-slip faults on Europa (see Fig. 2 for locations), with geologic interpretations for each fault type. Faults are shown in dark gray; offset features are shown in white. (a) Ridge-like strike-slip faults are ridges that show clear evidence of lateral offsets. This example from the south polar region (78.8° S, 121.7° W) exhibits 3.5 km of right-lateral offset of a relatively older ridge. (b) Band-like strike-slip fault with a smooth band internal morphology indicating little disruption of the fault zone material. This close-up view of part of Astypalaea Linea (68.6° S, 197.7° W) shows 77 km of right-lateral offset. The fault zone is cut by two relatively younger ridges. (c) Band-like strike-slip fault with a large amount of internal disruption of fault zone material. This close-up view of the eastern end of Agenor Linea (40.9° S, 186.5° W) shows about 1.2 km of right-lateral offset.

offsets are generally too small to resolve in Galileo images.

Nonetheless, many lineae on Europa exhibit lateral offsets of relatively older crosscutting features. These lineae commonly, but not always, resemble ridges (Fig. 1a) (e.g., 64% of examples in a study by Hoppa et al., 2000); however, the lateral motions along these ridges characterize them as strike-slip faults, which will thus be referred to here as *ridge-like* faults. Non-ridge-like lineae that exhibit lateral offsets across them typically have morphologies that closely resemble bands, meaning that the boundaries of the fault zone are up to several tens of kilometers apart and are separated by seemingly new crustal material within the fault zone. This fault zone material ranges in morphology from smooth and relatively undisrupted (Fig. 1b) to highly internally deformed (Fig. 1c). Strike-slip faults with either of these morphologies will be referred to as *band-like*. It is evident that the fault zone material represents new crust emplaced into the fault zone from below because offset features on either side of a band-like fault typically can be exactly

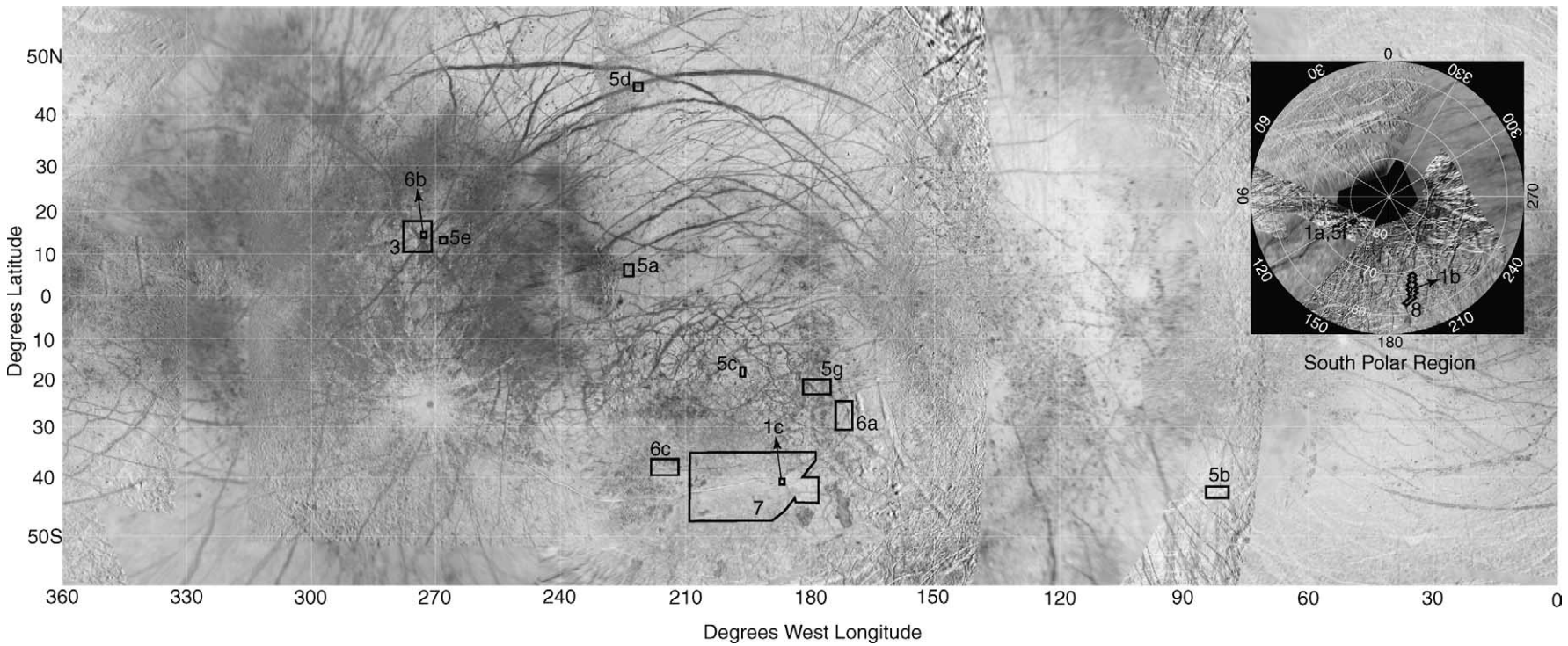

Fig. 2. Global map of Europa in mercator projection showing locations of all images used in this study. Inset: polar stereographic projection of the south polar region. The Galileo orbit number for the origin of each image is as follows (image resolution in parentheses in m/pixel): E6: Fig. 3 (182), 5e (182), 6b (21). E12: Fig. 5c (50). E14: Fig. 5g (240), 6a (240). E15: Fig. 5d (230). E17: Fig. 1a (41), 1b (43), 1c (50), 5a (220), 5b (240), 5f (41), 6c (220), 7 (220), 8 (43).

matched across the fault when reconstructed. This type of reconstruction is relatively simple along smooth band-like faults (Fig. 1b) but is commonly difficult along internally-disrupted band-like faults (Fig. 1c) (Prockter et al., 2000; Tufts et al., 2000; Greenberg, 2004).

Some strike-slip faults are several hundreds of kilometers in length (Fig. 2), analogous to major terrestrial strike-slip faults such as the San Andreas and North Anatolian faults. The Europan faults differ from their terrestrial analogs, however, in that the lateral offsets are typically on the order of a few tens of kilometers at most (e.g., ~ 20 km along Agenor Linea; Prockter et al., 2000) whereas comparably-sized terrestrial transform faults may exhibit offsets of hundred of kilometers. The greatest strike-slip offset documented on Europa thus far is 83 km (Sarid et al., 2002). Specific named examples of Europan strike-slip faults include Astypalaea Linea (Tufts, 1998, PhD thesis; Tufts et al., 1999; Greenberg and Geissler, 2002); Agenor Linea (Schenk and McKinnon, 1989; Geissler et al., 1998; Prockter et al., 2000; Kattenhorn, 2003); Corick Linea (referred to as "Agenor's Twin" by Greenberg, 2004), and Katreus Linea (Geissler et al., 1998; Greenberg, 2004). Each of these fault examples is band-like in appearance. In contrast, simple ridge-like strike-slip faults have not been rigorously studied, are typically at the smaller end of the length spectrum (a few tens of km), and may exhibit offsets of only a few hundred meters to a few km (Fig. 1a). Nonetheless, the longest lineae on Europa are typically complex ridges (also called ridge complexes; Figueredo and Greeley, 2004), which are comprised of numerous mutually adjacent or anastomosing ridges. Some ridge complexes have evolved into strike-slip faults with lateral offsets as large as those along band-like faults (e.g., the 83-km-offset example of Sarid et al., 2002). Such large offsets along ridge complexes are not the rule, however. For example, Agave Linea (Fig. 3) is at least 2000 km long but has undergone only ~ 5 km of left-lateral offset near Conamara Chaos. The entire length of Agave Linea was not captured in high resolution Galileo images; therefore, unlike many terrestrial fault analyses, it is not known how strike-slip offsets vary along the entire length of this, or any analogous, feature.

The majority of the previous studies of strike-slip faults on Europa have been description-based, providing details about locations, orientations, maximum offsets, shear sense, and internal morphology (Hoppa et al., 1999a, 2000; Tufts et al., 1999; Prockter et al., 2000; Sarid et al., 2002; Figueredo and Greeley, 2004). Other than a few studies that have acknowledged the possibility of shear failure of intact Europan ice in the existing tidal stress field (Schulson, 2002; Spaun et al., 2003; Kattenhorn, 2004), there have been no investigations into the mechanical development of strike-slip faults, such as their initiation and subsequent growth. The most viable existing hypothesis for strike-slip fault behavior on Europa (after the fault has already formed) is the tidal walking theory (Hoppa et al., 1999a), which predicts the sense of offset along strike-slip faults in the context of global tidal

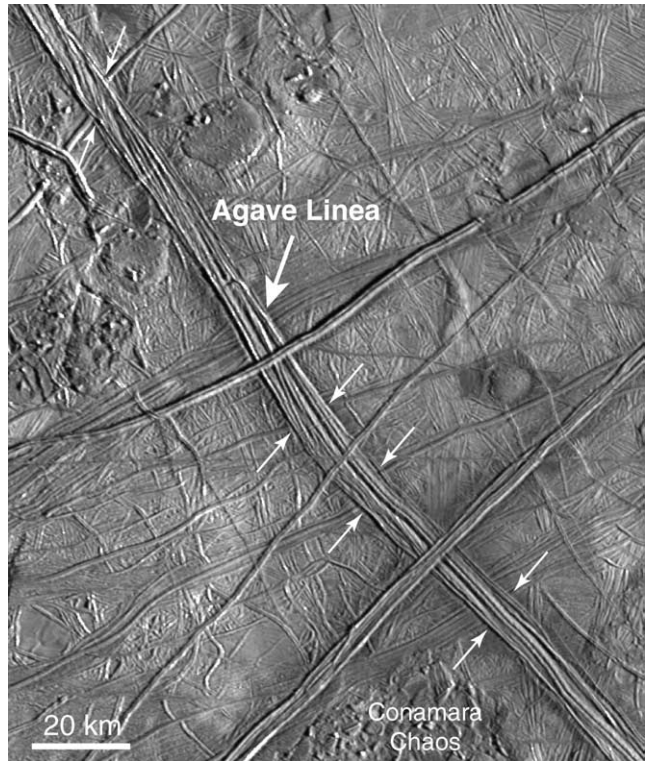

Fig. 3. A 195-km-long portion of Agave Linea near where it passes alongside the northeastern edge of Conamara Chaos (image centered at 14.1° N, 273.6° W). Agave is a ~ 2000-km-long ridge complex that exhibits left-lateral offsets (marked by small arrows), making it a ridge-type strike-slip fault. Compared to the length of the ridge complex, offsets are small (maximum visible is ~ 5 km) and vary in magnitude along the length of the fault.

stresses. The theory suggests that fault motions are driven by diurnal tidal stresses (Greenberg et al., 1998), which rotate in a relatively opposite sense in the north and south hemispheres. In essence, the changing magnitudes of the rotating stresses result in a recurring cycle of fault dilation with frictionless forward shear motion, followed by closing and a lesser amount of frictional backward shear motion. The overall result is that strike-slip faults accumulate displacements over time like a ratchet, with a preponderance of left-lateral offsets in the northern hemisphere and right-lateral offsets in the southern hemisphere (with variations dependent on fault orientation within 30° of the equator), in agreement with observed offsets along large faults (Hoppa et al., 1999a; Sarid et al., 2002).

Although the tidal walking theory does seem to explain the observed offset sense along many large faults, these offsets only provide indirect support of the theory. In other words, the offsets are compatible with the tidal walking theory, but do not provide irrefutable evidence of its occurrence, such as would be provided by direct mechanical confirmation of the hypothesized cycle of fault behavior during the diurnal cycle. To examine this problem, I use a different line of evidence to investigate the mechanics of strike-slip fault evolution on Europa: secondary fracturing at the tips of

strike-slip faults in the form of tailcracks. The geometries of tailcracks provide a direct signature of the mechanics of fault motions and can thus be used to test the tidal walking theory as well as providing insights into the fault growth process on Europa. I present observations of tailcrack geometries along Europan faults (Section 2) and compare them to the results of analytical stress models (Section 3) to show that strike-slip fault motions commonly included a significant component of opening motion. However, fault dilation is characteristic of band-like faults, not ridge-like faults, implying that tidal walking may not necessarily describe the slip behavior of all strike-slip faults on Europa.

2. Tailcracks on Europa

2.1. What are tailcracks?

On Earth, it is common to observe typically curved secondary tension fractures alongside slipping interfaces and faults which, depending on exact morphology, have been termed tailcracks, wing cracks, kinks, or horsetail fractures (Cruikshank et al., 1991; Willemse et al., 1998). These secondary fractures, henceforth referred to exclusively as tailcracks, typically form on one side of the tip of a slipping fault (Fig. 4a) or around small jogs, steps, or other complex-

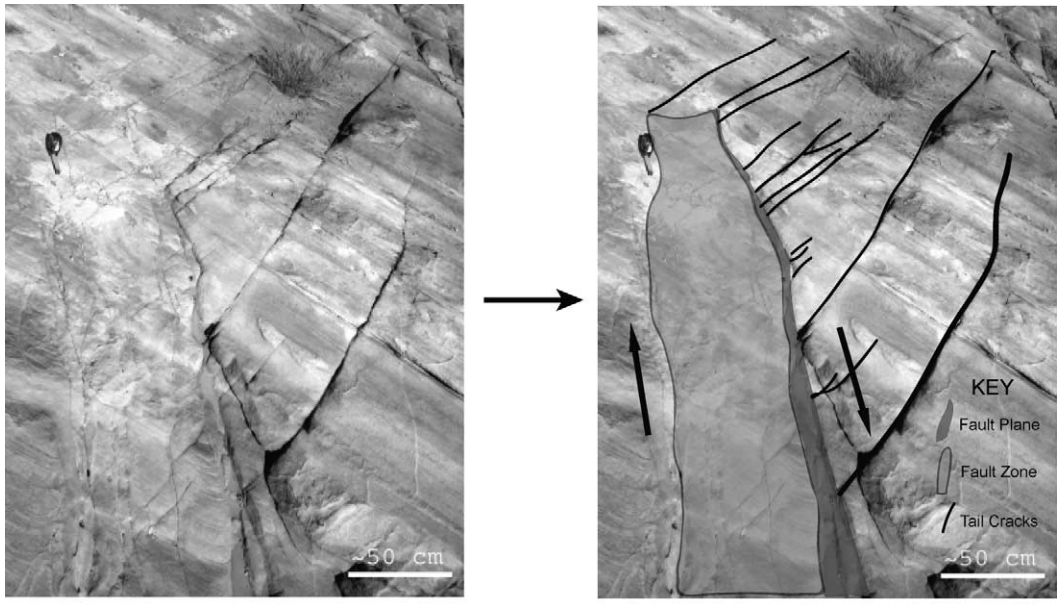

(a)

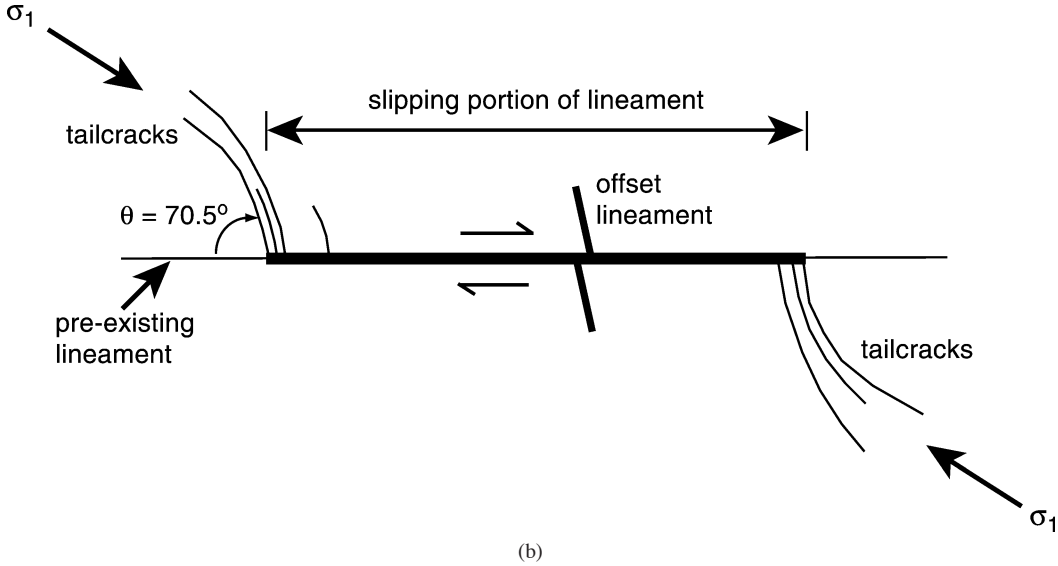

(b)

Fig. 4. (a) Oblique view of tailcracks emanating away from the tip of a right-lateral fault in sandstone, Valley of Fire State Park, Nevada. The fault zone (shaded) is 85 cm wide and has undergone a few centimeters of slip along the main slip plane (dark gray). The tailcracks are oriented at 70° to the strike of the fault. (b) Theoretical geometry and antisymmetric distribution of curved tailcracks at the ends of a slipping portion of a preexisting lineament (right-lateral case). For pure strike-slip motion (mode II) with no concurrent opening, tailcracks form with a tailcrack angle of $\theta = 70.5°$ with respect to the fault and then curve towards the σ_1 direction. The left-lateral case is the mirror image of this diagram.

ities along a fault surface. Tailcracks form an antisymmetric pattern at opposite tips of the fault (Fig. 4b), although they do not necessarily form at both tips. The fracture geometry at any fault tip is a mechanical indicator of the sense of slip and can thus be used to determine if fault motion is left-lateral or right-lateral (Pollard and Aydin, 1988; Cruikshank et al., 1991), which can be useful in the absence of relative-offset indicators. The intersection of the tailcrack and the fault plane is typically manifested as a sharp kink, quantified using the tailcrack angle (θ in Fig. 4b). Nonetheless, the intersection of a fault and a secondary crack is sometimes curved rather than kink-like. Such a geometry at the tip of a slipped interface is called a veer and indicates that crack growth occurs as the interface is progressively sheared (Cruikshank et al., 1991). Thus, veering results in a new orientation of cracking in response to lateral motion along a fault. As with tailcracks, the differently-oriented, new crack growth is typically in the form of a tension crack as opposed to the shear-crack nature of the fault itself. For this reason, a secondary crack caused by a veer, rather than a sharp kink, will also be referred to here as a tailcrack, with the tailcrack angle representing the change in orientation of the fault in the zone of veering. In such cases, lateral offsets must be identified along the fault to differentiate this crack geometry from that of a tension fracture that grew with a curved shape in a spatially variable stress field.

Tailcracks develop in response to concentrations of stress around the periphery of a slipping fault. The orientations of these perturbed stresses differ from the regional stress orientations responsible for fault slip, causing tailcrack orientations to be at an angle to the plane of the primary fault. The shape of the tailcracks is controlled by the spatial variability in the stress field at the fault tip, which, in turn, is controlled by the remote state of stress and the specifics of fault motion (Pollard and Segall, 1987; Lawn, 1993; Kattenhorn, 2002). For example, if the fault surfaces remain in contact during slip, tailcracks are predicted to form at a 70.5° angle with respect to the primary fault strike, then curve away from the fault towards the direction of the maximum compressive principal stress, σ_1. This growth behavior results in curved tailcracks, concave towards the regions beyond the fault tips (Fig. 4b). Tailcracks may be relatively straight where the stress field is less spatially variable, such as in a relay zone between overlapping fault segments that may or may not be linked by the tailcracks (Crider and Pollard, 1998; Kattenhorn et al., 2000), or where the tailcrack dimensions are smaller than the extent of the perturbed stress field around the fault tip. Tailcracks are typically much shorter than the faults that formed them; nonetheless, tailcracks can eventually exceed the length of the fault at which they initially formed as long as sufficient driving stress exists for continued growth, particularly if the tailcracks experience a large crack-parallel compressive stress (Nemat-Nasser and Horii, 1982; Granier, 1985; Koenig and Aydin, 1998; Kim et al., 2001).

2.2. *Tailcracks along Europan strike-slip faults*

The identification of strike-slip faults on Europa has also led to the recognition that some fractures in the ice shell are not caused primarily by global tidal stresses but are, in fact, secondary tailcracks resulting from lateral motions along strike-slip faults (Schenk and McKinnon, 1989; Schulson, 2002; Kattenhorn, 2003). These tailcracks are not uncommon and have previously been described at the tips of band-like strike-slip faults; however, as is indicated below, this seeming prevalence along band-like faults simply reflects the fact that simple ridge-like faults tend to be relatively shorter with small tailcracks that are sometimes difficult to identify against the background of ridged plains. In actuality, tailcracks are also very common along ridge-like faults. A survey of tailcracks across all regions of Europa imaged by the Galileo spacecraft (Fig. 2) has indicated a wide variability of tailcrack angles with respect to fault strike, ranging from 30° to 80°. It is therefore important to examine the specific conditions under which tailcracks developed on Europa in order to interpret the mechanics of their formation and explain their common dissimilarity to terrestrial tailcracks (Fig. 4).

The remainder of this paper will demonstrate the importance of these tailcracks for revealing details about the nature of the stress field that existed at the time of fault motion. Ridge-like and band-like fault styles will be considered separately in order to highlight differences between tailcrack development associated with each type of faulting and the significance of this for unraveling details of the fault evolution. In each fault example presented here, evidence for strike-slip motion is provided in the form of lateral offsets of preexisting features. These offsets are not apparent offsets caused by dilation or compression along the fault, based on the following logic: (1) It is impossible to cause lateral offsets through fault-perpendicular dilation alone (regardless of the obliquity of the preexisting feature); therefore, even where evidence of fault dilation exists, lateral offsets imply a component of strike-slip motion accompanied dilation. The term oblique dilation could be applied to such a scenario, but this term is reserved to cases of reactivation of an old fault by later plate spreading and so will not be used here in order to differentiate primary fault motion from later spreading effects. (2) Contraction across a fault prevents features from being accurately matched from one side of the fault to the other during fault reconstructions as a result of material being consumed within the fault zone by the contraction (e.g., Greenberg, 2004). In every example presented here, features can be matched up across the fault, indicating that offsets are not due to any appreciable contraction along the fault. It should be noted that the mere presence of a tailcrack at the tip of a fracture can be used as evidence of lateral motion along that fracture; nonetheless, at least one offset feature is shown for each example presented here to prove that lateral motion has indeed occurred and that the sense of motion

is consistent with the tailcrack geometry with respect to the fault tip.

Tailcrack angles are measured only on high-to-medium resolution (21–240 m/pixel) images in which the intersection of faults and tailcracks is clearly resolvable. Both mercator and orthographic reprojected images were used to make tailcrack angle measurements, justified by a comparison test of these reprojections of individual Galileo images (reprojected about the image center) that indicate accurate preservation of angular relationships to within a few degrees at the scale of the utilized images. This amount of inaccuracy is likely to exist for any tailcrack angle measurement, regardless of the type of reprojection, purely in response to image resolution constraints. For the purposes of this study, inaccuracies in tailcrack measurements of $< 10°$ do not impact on the general conclusions presented.

2.3. Ridge-like faults

Seven examples of tailcracks associated with ridge-like strike-slip faults are shown in Fig. 5. For each example, both an original image and a geologically interpreted image are shown, with faults indicated in blue, tailcracks in red, and offset features in various shades of green. These fault examples span a wide range of image resolutions (41–240 m/pixel) and geographic locations (from 45° N to 79° S, and from 76° to 269° W), with fault lengths ranging from as little as 12 km to more than 170 km within the limits of the imaged portions of the faults. The amount of offset across these faults ranges from about 450 m to 27 km, with no clear pattern of displacement distribution (i.e., displacements are not necessarily constant along any particular fault). Both left-lateral and right-lateral examples are shown, with no characteristic sense of offset in either hemisphere. As a result of resolution constraints, offsets smaller than a few hundred meters are imperceptible in even the highest resolution images. Nonetheless, it is clear that tailcracks many kilometers in length can develop along faults that have only slipped by a few hundred meters.

The morphology of the ridge-like faults varies from trough-like in appearance (poorly-developed raised rims along the fault; Figs. 5c and 5f) through distinctly ridge-like (exhibiting well-developed ridges to either side of the central crack; Figs. 5a, 5b, 5d, and 5e) to a morphology resembling a superposed ridge complex (large fault in Fig. 5f). The faults illustrate a range of tailcrack characteristics, both geometrically (in terms of the intersection angle with the fault, as indicated in Fig. 5) and morphologically (in terms of their general appearance in images). Tailcrack angles vary from 30° to 73° with an average of 54° and a median of 53° for sixteen measurements. These angles were measured directly from the images at the intersection point with the fault to circumvent errors introduced by changing tailcrack orientations with increasing distance from the intersection point. Tailcrack morphologies have a similar variability to faults, resembling one of three types of features: troughs, ridges, or bands. Tailcrack morphology is independent of the tailcrack angle and may or may not be the same as the fault that produced it; therefore, a change in morphology from a fault to a tailcrack is not the defining characteristic of a tailcrack. Rather, tailcrack development is indicated by an abrupt change in fault orientation (usually at a sharp kink) in response to lateral motion along the fault. Tailcracks can be differentiated from faults in that they lack lateral offsets when they first form, no matter what their morphology (i.e., they are tension fractures).

The example in Fig. 5a shows a 36-km-long, N–S striking right-lateral fault (6 km of offset) with a band-like tailcrack at the south tip exhibiting dilation vectors that are parallel to the fault motion vector. At its northern end, the fault curves towards the east and has thus dilated, becoming band-like, in response to slip at the southern end. The tailcrack at the southern tip makes an angle of 67° with the fault, is significantly longer than the fault that formed it, and curves into a different orientation with increasing distance from the fault tip, analogous to the theoretical example in Fig. 4. This fault resembles a cycloid (Hoppa et al., 1999b) and it is possible that it formed as such in this particular location. However, the geometry of the feature is distinctly non-cycloid-like outside the bounds of Fig. 5a. To the south, the feature changes into a $\sim$ 325-km long, zigzagging ridge. To the east, the fault continues for over 100 km with an unchanging E–W orientation before curving southwards again for hundreds of kilometers (as seen in low-resolution Galileo images), which would not be expected of a cycloid. Therefore, the general geometry of the feature at the location in Fig. 5a, combined with the fact that the slip vectors are perfectly parallel to the fault segment, justifies the interpretation of this example as a fault-tailcrack feature. It has been suggested that the fault motion is part of a larger scale plate rotation phenomenon in this region (Patterson and Head, 2004). Nonetheless, cycloid growth has also been hypothesized to be the result of tailcrack initiation at each cycloid cusp due to shearing of the most recent cycloid segment (Marshall and Kattenhorn, 2004); therefore, a cycloidal origin for the fault in Fig. 5a would not be problematic in terms of illustrating tailcrack development at the tip of a slipped fault segment.

In Fig. 5b, two short (20 and 30 km), NE–SW striking right-lateral fault segments (900 m of offset) have developed trough-like tailcracks at each of their respective tips. One of these tailcracks links the two faults together at their proximal tips, intersecting both faults at about 50°. The tailcracks at the distal ends of each fault formed at lower angles to the faults (34° and 30°, respectively). Both of these lower angle tailcracks are many times longer than the lengths of the faults themselves.

The tailcrack in Fig. 5c is imaged at 50 m/pixel resolution, allowing the details of the fault-tailcrack intersection to be observed in impressive detail. This 23-km-long, NNW–SSE striking right-lateral fault (600 m of offset) has not developed raised ridges alongside the fault and thus resembles a trough. The tailcrack is also trough-like, forms a 70° angle

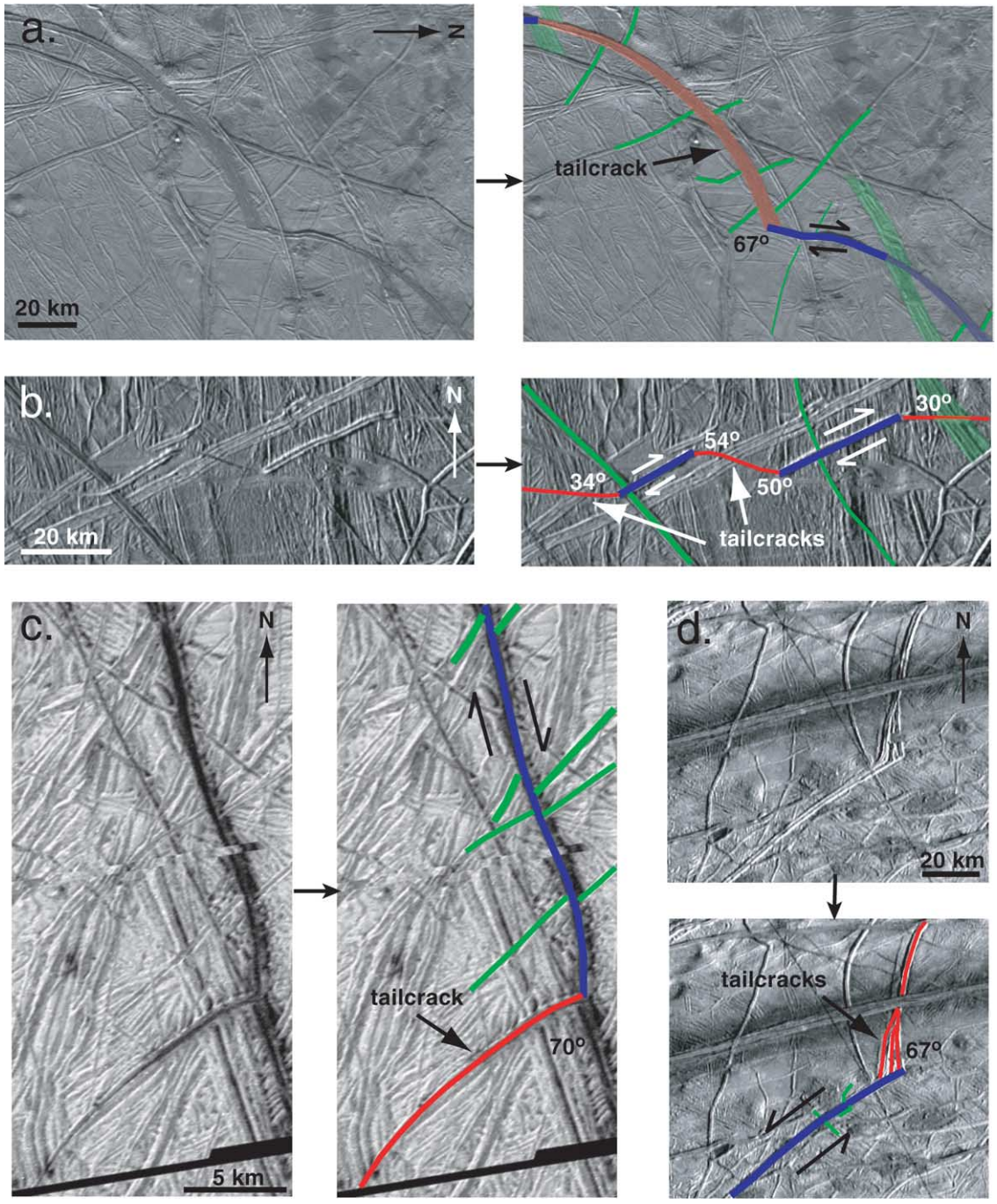

Fig. 5. Examples of tailcracks associated with ridge-like strike-slip faults. In each corresponding geologic interpretation, faults are shown in blue, tailcracks in red, and laterally offset, older features are shown in green. Tailcrack angles are as indicated. (a) A 36-km-long right-lateral fault at 5.2° N, 223.9° W. Maximum offset is 6 km. Motion along the fault has caused dilation and band development along the tailcrack. Dilation has also occurred along the northern, curved portion of the fault. (b) Two < 30 km-long right-lateral faults at 42.3° S, 76.4° W. Both faults exhibit tailcracks, one of which has linked the faults together. Maximum offset is ~ 900 m on the longer fault. (c) A right-lateral fault at 17.8° S, 196.7° W. Maximum offset is ~ 600 m. (d) A left-lateral fault with several tailcracks at 45° N, 222.4° W. A likely offset of ~ 2 km is indicated; however, crosscut features are difficult to correlate with certainty at the resolution of this image. (e) Right-lateral fault with two tailcracks at 12.5° S, 269° W. The maximum offset is difficult to estimate at this image resolution, but appears to be ~ 700 m. (f) Two left-lateral faults at 78.8° S, 121.7° W. The larger fault (top right) is a well developed ridge (maximum offset is 1.25 km). The smaller fault has been obscured by a younger trough (maximum offset is ~ 450 m). A younger right-lateral fault has offset both left-lateral faults. (g) Right-lateral fault in Argadnel Regio at 22.8° S, 177.2° W. Maximum offset is 27 km. Motion along the fault is accommodated by dilation and band development along the tailcracks.

with the fault, and curves away from the fault tip, again analogous to Fig. 4. In Fig. 5d, several tailcracks are clustered at the northern tip of a left-lateral fault that has undergone about 2 km of offset, although this estimate may be inaccurate as a result of the resolution of the image (230 m/pixel). The tailcrack angle at the tip of this fault is 67° whereas the

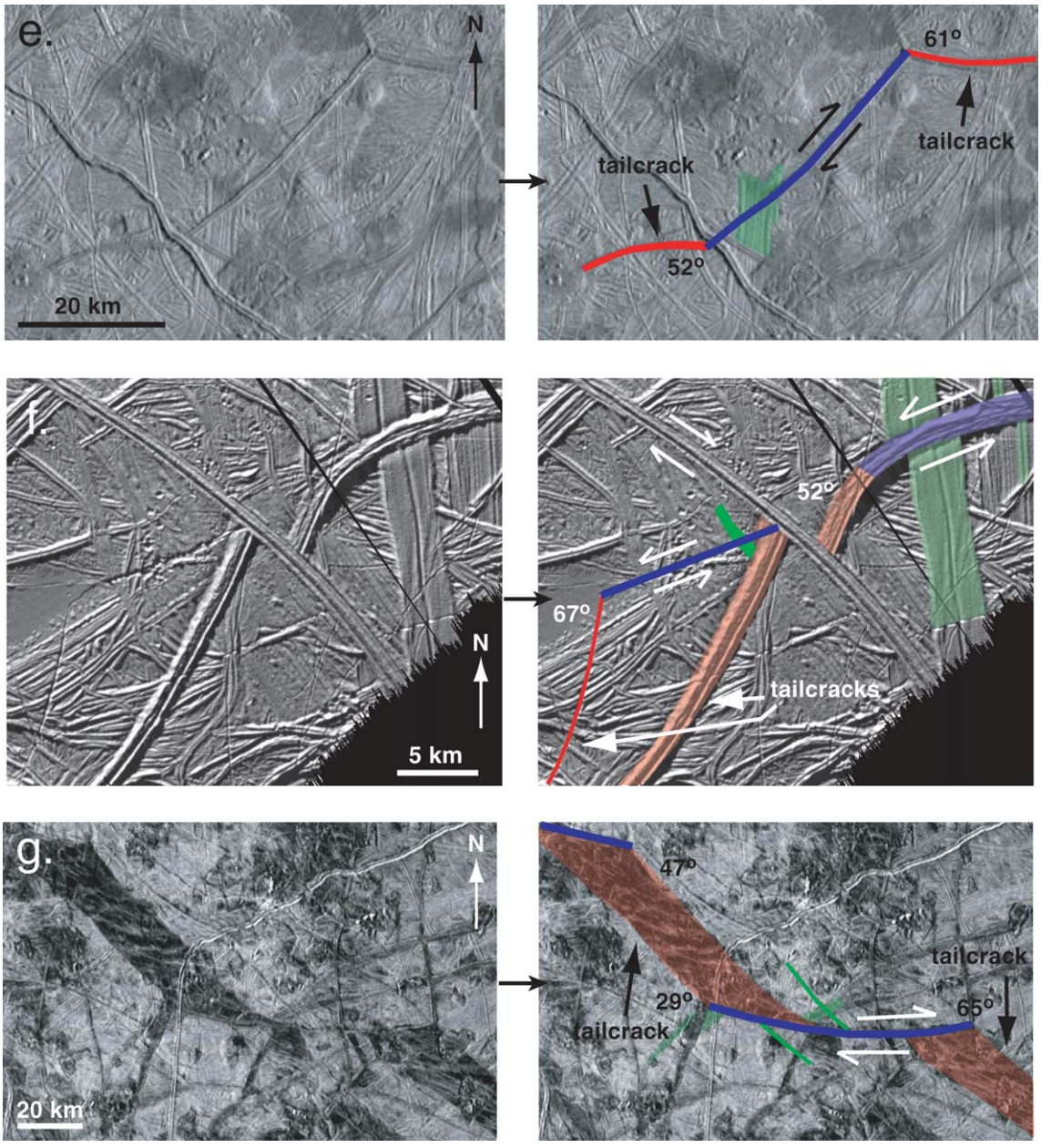

Fig. 5. Continued.

other two tailcracks appear to have formed at lower angles to the fault (50°–60°), although these angle estimates are less reliable due to the superimposition of several ridge-like tailcracks in this vicinity. The 40-km-long, NE–SW striking right-lateral fault (700 m of offset) in Fig. 5e has developed ridge-like tailcracks at both fault tips, forming intersection angles of 52° and 61°, respectively.

In Fig. 5f, two distinctly different fault-tailcrack geometries and morphologies occur in close proximity to each other. The larger, ENE–WSW striking fault resembles a ridge complex with a clearly discernible 1.25 km of left-lateral offset. It is clear that the abrupt change in orientation of the fault in this location is a response to the left-lateral motion, causing a ridge-like tailcrack to develop at the western tip at an approximate angle of 52° to the fault. The intersection of the fault and the tailcrack is more curved than kink-like and is thus a veer. Nonetheless, the fairly abrupt change in fault orientation characterizes this feature as tailcrack-like. The tailcrack angle was approximated by comparing the general trends of the fault and the tailcrack in the vicinity of the sudden veering. The tailcrack was later cut and offset by a younger right-lateral fault. Also observable in Fig. 5f is a 15-km-long, ENE–WSW striking left-lateral fault (450 m of offset) that appears trough-like but may be a ridge that has been obscured by the development of a younger trough along its margin. The tailcrack is trough-like and makes a 67° angle with respect to the fault.

Finally, in Fig. 5g, a distinctly different fault-tailcrack morphology is shown from the "Wedges" region (now officially called Argadnel Regio), which has previously been documented for its plentiful band-like spreading features (Schenk and McKinnon, 1989; Schulson, 2002). This region contains a number of long (10s of km) fault segments that are typically linked by dilated bands that formed as tailcracks at the fault segment tips. In this 240 m/pixel resolution image, the 82-km-long, E–W striking, seemingly ridge-type fault has undergone 27 km of right-lateral offset, mostly accommodated by the dilation of two band-like tailcracks at each tip. The eastern tailcrack formed at 65° to the fault whereas the western tailcrack intersects the fault at 29°, linking the fault to a second fault segment to the northwest, which forms a 47° angle with the linking tailcrack. The faults and tailcracks in this example have been superposed with numerous crosscutting ridges and other deformation features, indicating that the fault may be a particularly ancient example in the observable geologic sequence.

2.4. Band-like faults

Three examples of tailcracks associated with band-like strike-slip faults are shown in Fig. 6. Additional case examples in Fig. 7 (Agenor Linea) and Fig. 8 (Astypalaea Linea) will be described in greater detail in the following sections. Band-like fault-tailcrack relationships are visible across a wide range of image resolutions (21–240 m/pixel) and geographic locations (from 15° N to 79° S, and from 170° to 273° W). In the examples presented here, fault lengths range from 12 km to about 1500 km. For the case of band-like faults, fault zone width (or thickness) becomes a prominent feature and ranges from about 400 m (Fig. 6b) to as much as 55 km across the width of Astypalaea Linea (Fig. 8a). The amount of offset across these faults ranges from about 280 m to 56 km. The single left-lateral example shown is in the northern hemisphere whereas all the southern hemisphere examples are right-lateral faults. Tailcrack angles vary from 14° to 80° with an average of 37° and a median of 30° for ten measurements associated with band-like faults with internally deformed morphologies (Fig. 1c) (i.e., excluding Astypalaea Linea; Figs. 1b, 8). These angular relationships imply that typical tailcracks along band-like faults form at angles to the fault strike that are $> 20°$ smaller than along ridge-like faults. As will be discussed later, there are important mechanical reasons based on structural reconstructions as to why Astypalaean tailcracks should be considered separately from other band-like faults.

The first band-like fault example (Fig. 6a) is from Argadnel Regio, similar to the ridge-like fault example in Fig. 5g. In contrast to the latter example, however, the 82-km-long, NW–SE striking right-lateral fault shown in Fig. 6a (25 km of offset) exhibits a 4-km-wide fault zone containing infill material analogous to the dark material that was emplaced into the dilated tailcracks at each tip of the fault. The tailcrack at the southern tip makes a relatively high angle of 80° to the fault but the northern tailcrack intersects the fault at about 55°. The northern tailcrack links the fault to an adjacent fault segment to the northwest, but the southern tailcrack extends for a distance of 130 km from the fault tip, gradually thinning to a sharp end-point but lacking the curvature present in many of the ridge-type fault tailcracks in Fig. 5 as well as the theoretical example in Fig. 4b.

The fault in Fig. 6b occurs in the Bright Plains region, north of Conamara Chaos (Fig. 2). This 12-km-long, E–W striking left-lateral fault (280 m of offset) is perceptibly band-like in the 21 m/pixel resolution images (Kattenhorn, 2002), despite its very narrow width ($\sim$ 400 m at its widest point). Towards its western end, the fault seems to transition into a more trough-like morphology. The eastern tip of the fault contains a $\sim$ 3.4 km long ridge-like tailcrack that formed at a low angle to the fault ($\sim$ 18°) and, similar to the example in Fig. 5f, does not contain a sharp kink but rather a more gentle veering from the fault into the tailcrack. Nonetheless, the left-lateral motion along the fault is clear and is consistent with the sense of veering (to the left); therefore, this feature has been characterized as tailcrack-like.

A similar situation occurs at the western end of a segment of Katreus Linea (Fig. 6c), a prominent ESE–WNW striking bright band (up to 7 km wide) in the antijovian southern hemisphere. The portion of Katreus Linea shown here is $\sim$ 215 km long and represents the easternmost quarter of the entire length of Katreus. Careful matching of offset features in the somewhat homogeneous plains surrounding Katreus (imaged at 220 m/pixel resolution) indicates right-lateral offsets of about 27 km. In response to this right-lateral motion, a 52-km-long band-like tailcrack has developed on the northern side of the western tip of the fault. This tailcrack intersects the fault at 54°, although the exact nature of the intersection of the fault and the tailcrack has been somewhat obscured by the development of a triangular band-like triple-junction where an adjacent fault segment has intersected the fault. Nonetheless, the tailcrack is clearly observable curving towards the north away from the western tip of the fault. Note that the curvature of the tailcracks in both Figs. 6b and 6c is convex towards the direction beyond the fault tips. This sense of curvature is contrary to each and every tailcrack along the ridge-like faults in Fig. 5 as well as the theoretical examples shown in Fig. 4b.

2.5. Agenor Linea

Agenor Linea (Fig. 7) is the longest documented bright band on Europa, with a length of $\sim$ 1500 km (Prockter et al., 2000). This E–W striking right-lateral fault has been approximated to have undergone up to 20 km of offset and is up to 30 km wide. Its characteristics thus classify Agenor as a band-like strike-slip fault. Furthermore, Agenor exhibits at least six well-developed, trough-like tailcracks that curve towards the south at its eastern tip, which is compatible with right-lateral strike-slip motion. As a result of

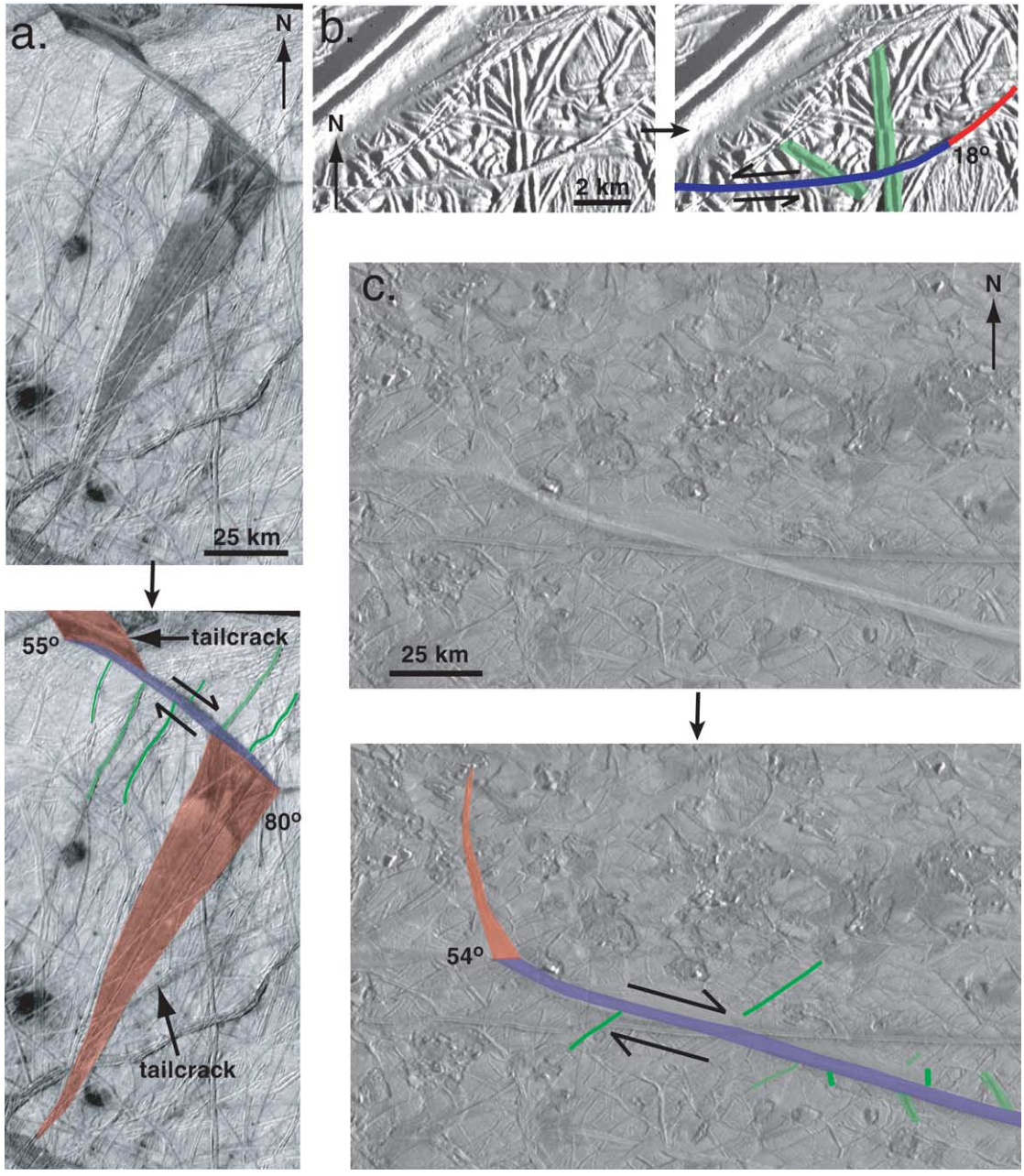

Fig. 6. Examples of tailcracks associated with band-like strike-slip faults. In each corresponding geologic interpretation, faults are shown in blue, tailcracks in red, and laterally offset older features are shown in green. Tailcrack angles are as indicated. (a) Dilated and infilled tailcrack in Argadnel Regio (26.9° S, 170.3° W). Total fault offset is about 25 km. (b) A 12-km-long left-lateral fault in the Bright Plains region (14.6° N, 273.4° W). Maximum offset is ~ 280 m. The curvature at the eastern end of the fault is a veering tailcrack (i.e., no sharp kink) that formed at a low angle to the fault. (c) Western end of a 215-km-long segment of Katreus Linea (38.2° S, 217.6° W), a bright band north of, and similar to, Agenor Linea. Maximum right-lateral offset in the region shown is ~ 27 km.

the medium resolution (~ 220 m/pixel) of regional images along Agenor, and disruption of faulted features, it is difficult to accurately match up features across the fault (Prockter et al., 2000). There appears to be at least 12 km of right-lateral offset within 130 km of the fault tip in Fig. 7b; however, there are also some features near the tip that exhibit little to no offset at the scale of the images, suggesting that displacement decreases rapidly towards the tip or that the fault history is more complex than simply being the result of offset accumulation by homogeneously distributed strike-slip motions.

The disrupted internal morphology of Agenor has been hypothesized to be the result of compressive duplexing at restraining bends along the southern margin, subsequent to plate separation and extension along the developing strike-slip fault system (Prockter et al., 2000). Subsequent shearing produced the brighter and geologically younger northern margin of the fault zone. The origin and morphology of

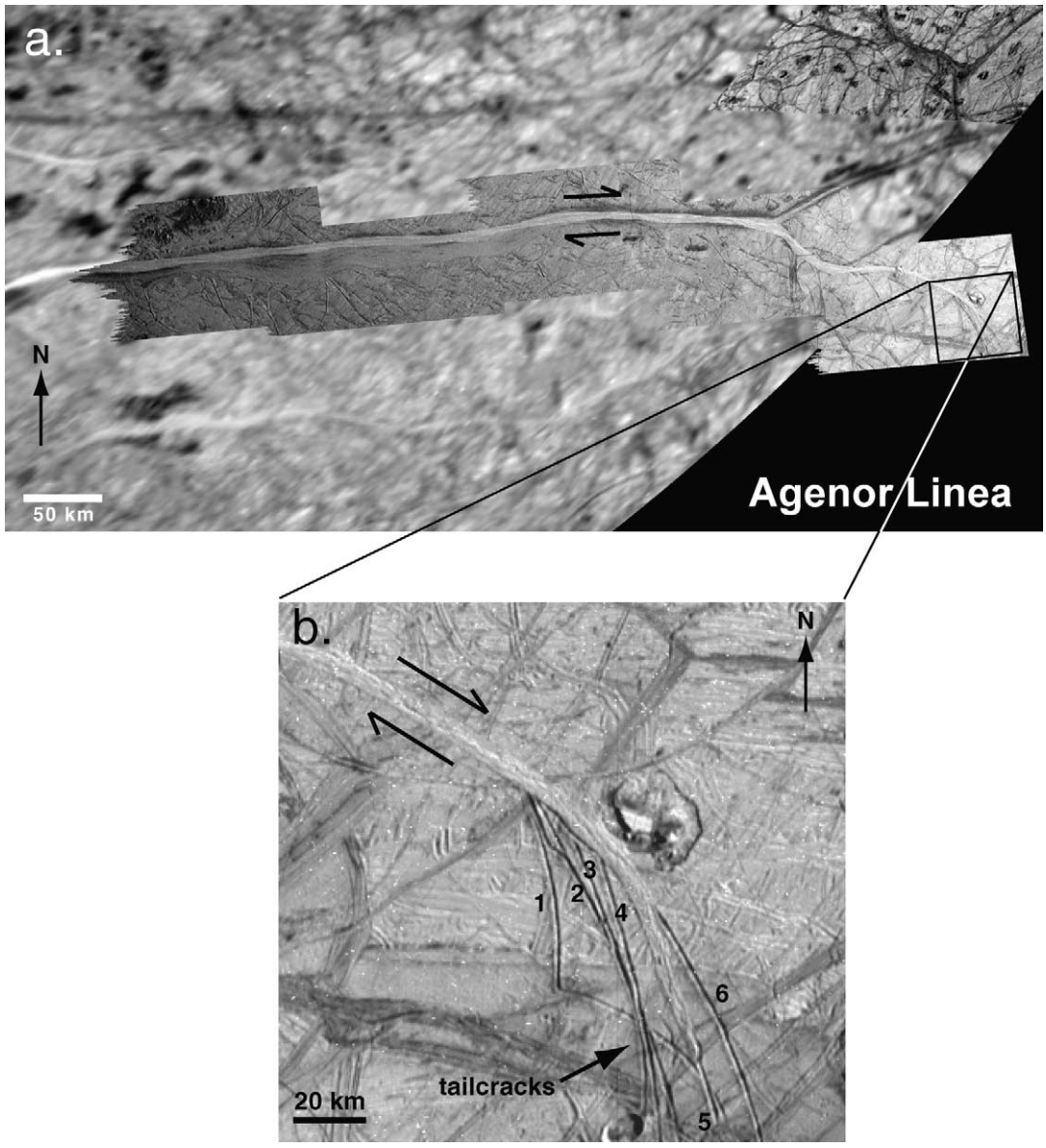

Fig. 7. (a) Agenor Linea, a ∼ 1500-km-long right-lateral strike-slip fault spanning from 170° to 250° W and from 37° to 44° S. The maximum offsets has been estimated to be ∼ 20 km (Prockter et al., 2000). (b) The fault geometry is irregular at its eastern end and is associated with numerous curved tailcracks. Crosscutting relationships suggest an eastward progression of tailcrack development (1 through 5; 6 is uncertain). The respective intersection angles of these tailcracks 1–6 with respect to the fault are 30°, 33°, 30°, 30°, 30°, and 14°. The sense of curvature of the tailcracks is opposite to the theoretical tailcracks shown in Fig. 4b.

Agenor has also been suggested to be the result of compressive band development to accommodate broad-scale crustal extension in Argadnel Regio to the north (Schenk and McKinnon, 1989; Greenberg, 2004); however, Greenberg (2004) indicates that compression along Agenor is not incompatible with there having been strike-slip motions and dilation during portions of the geologic history of the fault. Geissler et al. (1998) suggest that Agenor is oriented correctly to be subject to extension in the tensional stress field induced by combined diurnal and nonsynchronous rotation stresses, and that the albedo of the fault zone material with respect to the surrounding plains may be indicative of relatively young ice within the fault and hence recent fault activity. Recent activity is also indicated by very few relatively younger crosscutting fractures.

In the vicinity of the tailcracks, Agenor has a gently curved NW–SE orientation (Fig. 7b) and the tailcracks propagated away from the fault at low angles to the fault strike (in the range 14°–33°). The orientations of the tailcracks are sufficiently different that five of the six cracks cross each other, allowing crosscutting relationships to be used to deduce the relative order of tailcrack development (numbered 1 through 6 in Fig. 7b). It can thus be determined that the tailcracks furthest from the fault tip formed first and that the most recent tailcrack is likely to be the easternmost one, at the current fault tip. Some of the tailcracks are disrupted

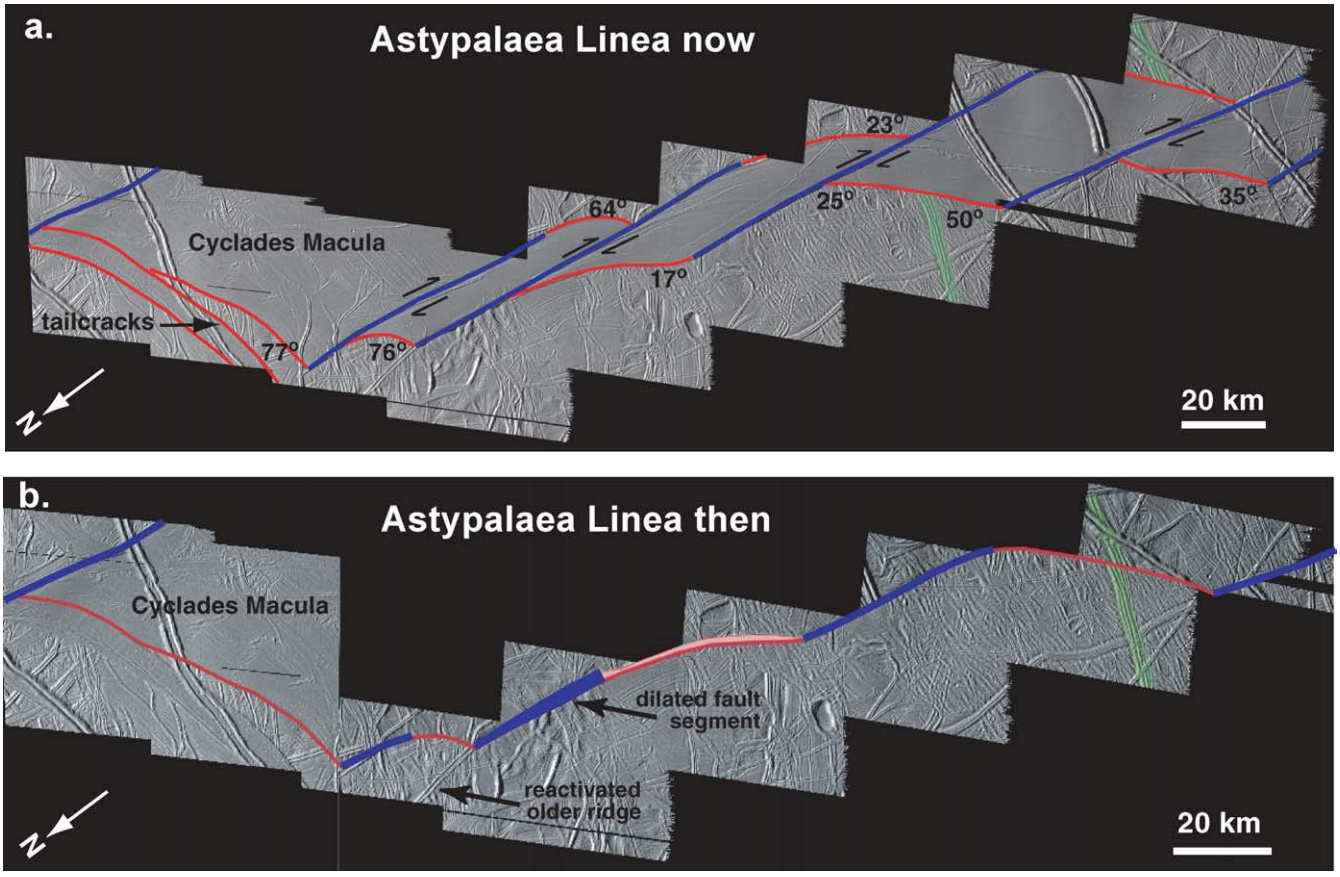

Fig. 8. (a) Northern end of Astypalaea Linea: an 810-km-long right-lateral strike-slip fault spanning from 60° S, 191° W to 79° S, 268° W (Tufts et al., 1999). This fault consists of a number of segments (blue lines) each of which underwent strike-slip motion. Smooth band material within the fault zone was produced in response to dilation along tailcracks (red lines), which formed at angles varying from 17° to 77°. Offsets in this portion of the fault (in green) are ~ 77 km (cf. Fig. 1b). (b) The original fault geometry can be conceptualized in this simple, rigid-block, structural reconstruction of the northern portion of (a), which matches up older crosscut features in the background plains. Cyclades Macula is not imaged in its entirety and so has not been reconstructed. The reconstructed fault implies some amount of initial dilation along the central fault segment, which is consistent with the low tailcrack angles at its southern end.

by chaos at the southern margin of Fig. 7b, indicating that chaos formation is more recent than tailcrack development in this region (cf. Figueredo and Greeley, 2004). The fault has utilized the fifth tailcrack to facilitate continued growth, indicated by bright band development along the trace of the crack. The oldest tailcrack (1 in Fig. 7b) exhibits an abrupt (~ 79°) kink along its trace, ostensibly due to a change in stress orientation after a pause in fracture growth. Cross-cutting relationships indicate that this kink and subsequent crack growth occurred prior to the development of later tailcracks, which may be indicative of a lull in fault activity between consecutive tailcrack growth episodes. During this lull, reworking of tailcrack 1 by diurnal tidal stresses may have induced kinking and crack reactivation analogous to suggested mechanisms of cycloid crack growth (Hoppa et al., 1999b; Marshall and Kattenhorn, 2004), or possibly in the form of a third-order tailcrack at the end of tailcrack 1. Finally, the geometry of the tailcracks is convex towards the region beyond the fault tip, analogous to the other band-like faults in Figs. 6b and 6c and dissimilar to ridge-like faults.

2.6. *Astypalaea Linea*

A final example of a band-like fault is Astypalaea Linea (Fig. 8a), which has an internal morphology reminiscent of smooth bands rather than being internally disrupted like Agenor and Katreus Linea (Figs. 6c and 7). Astypalaea has previously been documented (Tufts, 1998, PhD thesis; Hoppa et al., 1999a; Tufts et al., 1999; Mével and Mercier, 2002) as an 810-km-long right-lateral fault in Europa's southern polar region, spanning from 60°–79° S and 191°–268° W. A rigorous analysis of Astypalaea by Tufts et al. (1999) suggested that the fault underwent a consistent 42 km of right-lateral offset along its length; however, displaced features that can be matched up across the fault (green lineament in Fig. 8a) indicate a right-lateral offset of at least 56 km, suggesting that offsets are somewhat variable. Greenberg et al. (1998) indicate that Astypalaea was ideally oriented to have experienced combined dilation and right-lateral motion when it was situated about 20° west of its current location, before nonsynchronous rotation gradually reoriented the ice shell and moved Astypalaea into its current

longitudinal position. The smooth band material within the fault zone exhibits a finely lineated appearance defined by low-relief lineaments, some of which exhibit bilateral symmetry about the center of the smooth band, analogous to the mid-ocean ridge spreading-like mechanism hypothesized for dilational smooth bands on Europa (Prockter et al., 2002). The surface of Astypalaea is not heavily cratered and is overprinted by very few younger features (e.g., cycloid ridges), indicating a geologically young age for this particular fault.

A geologic analysis of the primary structural elements of the fault is shown in Fig. 8a, with fault segments traced in blue and tailcracks in red. The structural interpretation indicates that the fault is not a continuous linear structure (as appears to be the case with Agenor and Katreus Linea), but is rather composed of discrete N–S striking, right-lateral fault segments aligned along a NNE–SSW trend in a right-stepping en echelon pattern (cf. Tufts et al., 1999). Individual segments range in length from approximately 46 to 88 km in the region shown and exhibit a single raised rim suggestive of being one side of an initially ridge-like morphology despite the fact that the large-scale morphology of the fault at present is distinctly band-like. Each fault segment developed tailcracks at both tips in response to the right-lateral motion. The northern tip tailcracks thus propagated away from the fault segments towards the east whereas tailcracks at the southern tips propagated towards the west. These tailcracks facilitated the linkage of the fault segments to form a through-going fault structure. In this way, the developmental history of Astypalaea is similar to the faults in Argadnel Regio (Fig. 5g). Also analogous to those faults, dilation of the tailcracks along Astypalaea, such as can be determined from matching features across the fault (green lineament in Fig. 8), has accommodated the majority of the displacement along the individual fault segments and is thus ultimately responsible for the band-like nature of Astypalaea. Unlike the band-like faults described earlier (Section 2.4), therefore, the band-like appearance of Astypalaea resulted from dilation of the tailcracks, not dilation of the fault surfaces. It is for this reason that the tailcracks defining opposite edges of each individual smooth band are identical (Fig. 8a); they are the opposing sides of the initially juxtaposed tailcrack walls. This geometry suggests that the fault segments were linked by the tailcracks prior to dilation, as shown in the simple, rigid-block structural reconstruction in Fig. 8b. Individual tailcracks have perfectly linear edges with no flanking ridges, indicating that the initial morphology was likely trough-like rather than ridge-like.

Although dilation has occurred along the tailcracks in Fig. 8a, the angular relationships between the original (pre-dilation) tailcracks and the fault segments (Fig. 8b) have been preserved. There is a wide range of intersection angles between faults and tailcracks, ranging from 17°–77°. The tailcracks at the northern end of the fault define a broad smooth band region called Cyclades Macula and have intersection angles close to the theoretical 70.5° angle (Fig. 4b). The sense of curvature along these tailcracks is concave towards the direction beyond the fault segment tips, analogous to Fig. 4b as well as all the ridge-like faults in Fig. 5. The tailcracks with low intersection angles (17°, 23°, 25°, and 35°, respectively) are all curved in such a way that they are convex in the direction beyond the fault tips, analogous to the band-like strike-slip faults in Figs. 6 and 7. Some of these tailcracks then changed growth direction as they approached and ultimately intersected the adjacent fault segment.

3. Mechanical models of tailcrack development

Tailcrack orientations can be predicted analytically using principles of linear elastic fracture mechanics (LEFM), assuming that the faulted material is behaving elastically during the period of fault motion (e.g., Schulson, 2002). All fracturing on Europa has previously been interpreted to result from elastic stresses produced by reorientation of Europa's tidal bulges (Helfenstein and Parmentier, 1983, 1985; McEwen, 1986; Greenberg et al., 1998), indicating that application of LEFM to explain fracture orientations on Europa at the time scale of tidal deformation is quite typical. Ice has been documented to behave elastically under conditions of low temperatures, low confining pressures and high strain rates (Rist and Murrell, 1994). These conditions typify deformation of Europa's ice shell, which is subject to a constantly rotating diurnal stress field induced by the gravitational pull of Jupiter (Greenberg et al., 1998). It is thus not surprising that tailcrack features are observed along Europan strike-slip faults.

LEFM-based mechanical models have been applied to every style of fracturing on Earth (Jaeger and Cook, 1969; Pollard and Segall, 1987). Such studies have clearly demonstrated that the initiation orientations and propagation paths of fractures (such as tailcracks) are explicitly determined by the *mode* of fracturing, which is an LEFM nomenclature that describes the relative amounts of concurrent opening and sliding along a fracture or fault. Using this nomenclature, a tension-fracture (i.e., dilation only) is a mode I crack whereas a shear-fracture (i.e., sliding only, in the strike-slip sense) is a mode II crack.

For the case of isolated faults and fractures, simple analytical solutions exist to calculate parameters such as displacement profiles, elastic deformations, and stress magnitudes induced by the motions of the crack walls. I have extended such analyses to account for the sense of curvature of tailcracks, and thus describe the Europan crustal stress state at the time of fault motion as well as the physical behavior of the fault during slip events. Simple analytical solutions cannot account for mechanically-interacting faults; therefore, the effect of such interactions on tailcrack geometries (e.g., the shapes of tailcracks across linkage zones between adjacent fault segments; Figs. 5b, 5g, 8) is not addressed here. Nonetheless, even in such cases, the angle between a tailcrack and the fault that produced it is controlled by the near-tip stress field (and hence the specifics of motion along that

particular fault) and can thus be reasonably approximated with an isolated fault model as long as the overlapping faults are not closely spaced.

The stress tensor can be calculated at any arbitrary point in an elastic body containing a slipping discontinuity using the modified Westergaard stress functions (Pollard and Segall, 1987). Stress magnitudes and orientations are independent of the elastic properties of the body; therefore, direct comparisons can be made between terrestrial fracturing in rocks and Europan fracturing in ice. The generalized form of the crack stress function for any mode of crack motion is given by

$$\phi_m(z) = A_m\left[\left(z^2 - a^2\right)^{1/2} - z\right] + B_m z, \tag{1}$$

where the crack length is $2a$, m is the mode of failure (I or II), and z is the complex variable $z = x_2 + ix_1$. The crack is perpendicular to the x_1 axis and parallel to the x_2 axis in this formulation, and is centered about the center of the coordinate system. The constants A_m and B_m describe the nature of the loading of the crack for each respective failure mode, and are given by

$$A_m = [\Delta\sigma_{\mathrm{I}}, -i\,\Delta\sigma_{\mathrm{II}}] = \left[\left(\sigma^r_{11} - \sigma^c_{11}\right), -i\left(\sigma^r_{12} - \sigma^c_{12}\right)\right], \tag{2}$$

$$B_m = \left[\left(\sigma^r_{11} + \sigma^r_{22}\right)/2, 0\right], \tag{3}$$

where the r and c superscripts refer to the remote and crack components of the stress tensor, respectively. Commas separate the mode I and mode II solutions. The complex number i is equal to $(-1)^{1/2}$. For the two-dimensional case (a common simplification in LEFM), the components of the stress tensor are directly related to the crack stress function through the relationships

$$\sigma_{11} = \mathrm{Re}\left[\phi'_{\mathrm{I}}\right] + x_1\,\mathrm{Im}\left[\phi''_{\mathrm{I}} + \phi''_{\mathrm{II}}\right] - C, \tag{4}$$

$$\sigma_{12} = -\,\mathrm{Im}\left[\phi'_{\mathrm{II}}\right] - x_1\,\mathrm{Re}\left[\phi''_{\mathrm{I}} + \phi''_{\mathrm{II}}\right] - D, \tag{5}$$

$$\sigma_{22} = \mathrm{Re}\left[\phi'_{\mathrm{I}} + 2\phi'_{\mathrm{II}}\right] - x_1\,\mathrm{Im}\left[\phi''_{\mathrm{I}} + \phi''_{\mathrm{II}}\right] + C, \tag{6}$$

where Re and Im are real and imaginary parts of the complex functions, respectively, and the constants C and D are given by $C = (\sigma^r_{22} - \sigma^r_{11})/2$ and $D = -\sigma^r_{12}$. These stress tensor components can then be used to calculate the orientations of the maximum and minimum horizontal principal stresses (S_H and S_h, respectively, using a tension-positive sign convention) at any coordinate point (x_1, x_2) around a slipping or dilating crack (Pollard and Segall, 1987) using the equation

$$\alpha = 1/2\tan^{-1}\left[2\sigma_{12}/(\sigma_{22} - \sigma_{11})\right], \tag{7}$$

where α is the angle measured counter-clockwise from the positive x_2 axis to the direction of S_H. The direction of S_h is orthogonal to S_H.

By programming the above equations into the *Mathematica* software program, principal stress orientations were calculated in an elastic material around a slipping strike-slip fault, in order to approximate fault slip in Europa's ice shell and to make theoretical predictions about tailcrack geometries. Several loading conditions were considered, ranging from the pure strike-slip faulting case (mode II—no fault dilation), to cases where increasing fault dilation accompanied strike-slip motion (increasing mode I/mode II ratio). These loading conditions are predicated on the existence of commonly tensile tidal stresses in the Europan shell that may be important for fault dynamics (Hoppa et al., 1999a). The orientations of horizontal principal stresses are shown in Fig. 9 for the mode II case and for mode I/mode II ratios of 1, 2, and 3. In each example, the fault is right-lateral and is shown in blue; the left-lateral results would be the mirror image of those shown. Both distance axes are normalized to fault half-length, a, for ease of comparison with any fault of any length. Principal stresses are shown as orthogonal sets of gray ticks, with long ticks representing the greatest tension (S_H) and short ticks representing the greatest compression (S_h). Superimposed in red on these calculated stress fields are the predicted orientations and shapes of hypothetical tailcracks (mode I cracks) that would form in the fault-perturbed stress field at the fault tips. The lengths of tailcracks are for illustration purposes only; the lengths of actual tailcracks would depend on the availability of driving stress for continued crack growth. Note that LEFM predicts a stress singularity (i.e., infinite stress) at the tip of any slipping crack, regardless of its length or amount of slip. No brittle material can support an infinite stress; therefore, the material must respond by cracking, such as in the formation of tailcracks. For this reason, the model results are applicable to any fault on Europa, regardless of its size or distribution of slip. However, with increasing distance from the fault tip, stress orientations are clearly different depending on the relative amounts of sliding and opening, thus impacting on the geometry of the tailcracks that develop. Continued dilation of the tailcracks would help accommodate ongoing strike-slip motions along the fault and would result in the tailcracks developing a band appearance (regardless of whether the fault itself is ridge-like or band-like; Figs. 5a, 5g, 6a, 6c, 8a).

It can be seen in Fig. 9 that as the amount of fault dilation increases during concurrent strike-slip motion, the tailcrack curvature changes. The pure mode II case resembles many terrestrial examples, as idealized in Fig. 4b, with a fault/tailcrack intersection angle of 70.5° and a tailcrack curvature that is concave towards the direction beyond the fault tips. This particular case implies contact of the fault surfaces during slip events. However, with increasing fault dilation accompanying slip, tailcracks exhibit progressively smaller intersection angles with the faults and the sense of curvature eventually reverses to become convex towards the direction beyond the fault tips for mode I/mode II $\geqslant 2$. In addition, the tailcracks progressively rotate towards parallelism with the faults, but would never achieve parallelism as long as some element of mode II motion exists (Eq. (7)).

The implications of these model results as applied to tailcrack development on Europa are clear. Europan tailcracks exhibit a range of intersection angles with strike-slip faults, which can be explained as being the result of variable amounts of concurrent fault dilation and strike-slip mo-

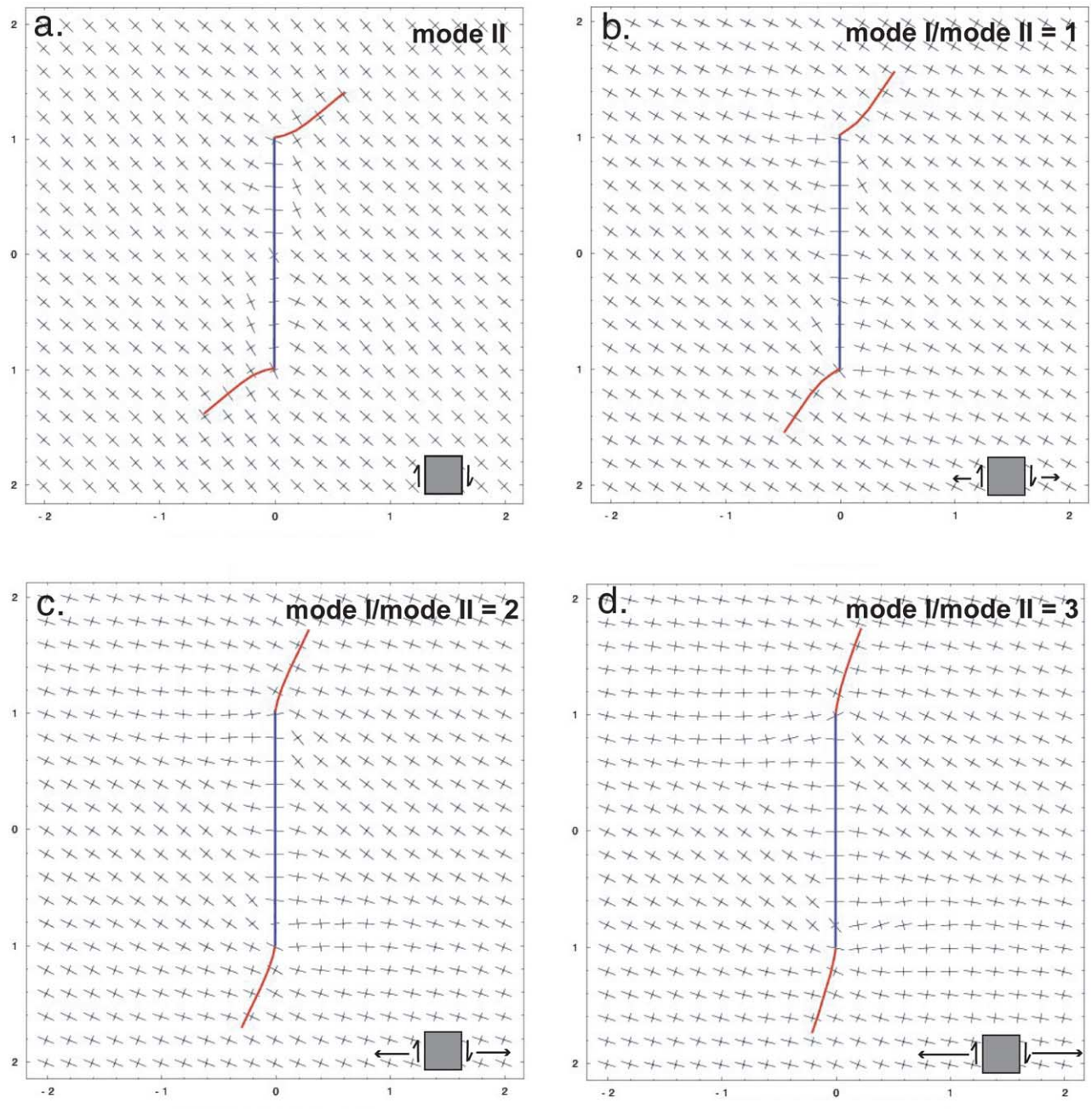

Fig. 9. Analytical model results of stress trajectories around strike-slip faults on Europa, showing the effect on tailcrack geometries of increasing fault opening during strike-slip motion (modeled as an increasing ratio of mode I to mode II loading as illustrated by the stress blocks in the lower right corner of each panel). All model results are for the right-lateral motion case; left-lateral results would be the mirror opposite. Long ticks represent the most tensile principal stress; short ticks represent the most compressive principal stress. Axis labels are in increments of crack half-length for ease of comparison with faults of any length. As the mode I/mode II ratio increases, tailcracks form at progressively lower angles to the fault and the sense of curvature reverses from the pure mode II case. Model results are shown for (a) pure mode II; (b) mode I/mode II = 1; (c) mode I/mode II = 2; and (d) mode I/mode II = 3.

tion at the instant of tailcrack development. Furthermore, the variable sense of curvature of Europan tailcracks (concave towards the direction beyond the fault tips in Figs. 5a–5g and some in Fig. 8a; convex in Figs. 6b–6c, 7, and some in Fig. 8a) can be directly correlated with the mode I/mode II ratio during fault motion and associated tailcrack growth. In the model results, lower intersection angles are coupled with convex curvatures, in agreement with Europan tailcracks. Most importantly, the fact that all examples of ridge-like faults with tailcracks described here (Fig. 5) have concave curvatures and higher median intersection angles implies that dilation is not a significant aspect of fault dynamics along these faults. Conversely, the fact that all but one of the band-like faults with tailcracks in Figs. 6 and 7 exhibit convex curvatures and low median intersection angles implies that dilation is a significant component of the dynamics

of band-like fault motions. For example, the tailcracks at the tip of Agenor Linea (Fig. 7) resemble the result for a mode I/mode II ratio of 2 (Fig. 9c), indicating twice as much tensile normal loading than shear loading driving the motions of the fault walls. This result implies that Agenor Linea was dilating at the time that tailcrack growth was occurring at its tip during fault slip. A similar conclusion may be drawn for Katreus Linea (Fig. 6c). Astypalaea Linea is somewhat anomalous in that it exhibits both high-angle/concave and low-angle/convex tailcracks along the same fault (Fig. 8a). This variability may indicate that some of the segments of Astypalaea underwent pure strike-slip motions whereas others underwent combined dilation and strike-slip motions, as suggested by the structural reconstruction of the fault (Fig. 8b).

4. Discussion

The large number of strike-slip faults that exist on Europa illustrate the importance of unraveling the nature of strike-slip fault initiation and evolution in order to fully understand the significance of lateral fault motions within the broader context of the geological deformation of the ice shell. Unfortunately, rigorous mechanical analyses of fault evolution are currently lacking, including the manner in which strike-slip faults accumulate slip over time. The tidal walking theory of Hoppa et al. (1999a) provides an elaborate driving mechanism for slip accumulation based on the theoretical global diurnal tidal stresses; however, tidal walking has been adopted as a general model for the behavior of all strike-slip faults on Europa, perhaps unjustifiably in light of the variability in fault characteristics presented here. There is a distinct possibility that strike-slip faults on Europa do not all slip in the same manner, but rather that different types of slip behavior exist as a function of location, global tidal stress state, ice shell thickness, and perhaps the mode of fault origin (primary shear failure versus reactivation of existing structures).

The tidal walking model predicts decoupling of the fault walls during a portion of the slip accumulation process and predicts a prevalence for right-lateral faults in the southern hemisphere and left-lateral faults in the northern hemisphere. This rule does not hold exactly true within $\sim 30°$ of the equator, where fault slip sense is also affected by fault orientation (Hoppa et al., 1999a). Furthermore, the slip sense of near-equatorial faults may have been impacted by some amount of polar wander (Sarid et al., 2002) as well as the effects of nonsynchronous reorientation of the ice shell since the time of fault activity. It is also possible that strike-slip motions, in some cases, are not driven by tidal stresses at all but rather represent accommodation of regional deformation or strike-slip motions along nearby faults. Nonetheless, all of the band-like faults described here are compatible with the predictions of tidal walking, yet the same is not true for ridge-like faults. For example, there are two left-lateral faults in the south polar region shown in Fig. 5f, yet tidal walking theory predicts only right-lateral faults at this latitude, regardless of longitude. Similar inconsistencies are indicated by Spaun et al. (2003).

Likely differences between the evolutionary history and slip accumulation dynamics of ridge-like versus band-like faults are also implied by the tailcrack geometries described here. Along ridge-like faults, tailcracks typically form at high angles to the strike-slip faults that produced them (Fig. 5), with few exceptions. Furthermore, these tailcracks consistently curve away from the faults in such a way that they are concave towards the direction beyond the fault tips. In this way, tailcracks along ridge-like faults are remarkably similar to tailcracks along terrestrial faults as well as the predictions of theoretical models that imply contact of the fault surfaces during fault slip (Fig. 4b). This behavior seems incompatible with tidal walking, which requires decoupling of the fault surfaces, and implies that the cumulative sense of slip is that which occurs during a dilational phase of fault motion. Some other mechanism driving the motion of the majority of ridge-like faults may thus exist, allowing the fault surfaces to remain in contact during slip accumulation and tailcrack growth, and thus perhaps allowing frictional shear heating along the walls of the fault to create buoyant upwelling of ice that assists in the construction of ridges (cf. Nimmo and Gaidos, 2002). The absence of a dilational phase also explains the lack of infill material within the fault zone. In some cases, tailcrack angles appear to exceed the theoretical 70.5° maximum. Such high angles may reflect the several degrees of potential error in angular measurements due to image reprojection or resolution constraints (true of all tailcrack measurements), but may also be an indicator of other mechanical effects such as the introduction of a vertical component of motion (e.g., Kattenhorn et al., 2000), frictional variability near the fault tip, or the effects of the preexisting structural fabric of the ice.

In contrast to ridge-like faults, tailcracks along band-like faults typically have low intersection angles with faults and the sense of curvature of the tailcracks is convex towards the direction beyond the fault tips (Figs. 6b, 6c, 7, and 8; Fig. 6a is discussed later). The analytical modeling presented here (Fig. 9) illustrates that such tailcrack patterns are consistent with concurrent fault opening and shearing. The band-like nature of the faults can thus be attributed to the emplacement of material into the fault zone from below during the dilational phase. The slip dynamics of band-like faults, as deduced from tailcrack geometries, is consistent with the tidal walking model and thus perhaps provides independent corroboration of the model with no exceptions to the predicted slip sense in any of the examples presented here.

Based on all of the observations presented in this study, two models of strike-slip fault evolution can be conceptualized. In the model for ridge-like faults (illustrated for the right-lateral case in Fig. 10a), fault surfaces remain in contact during slip episodes, producing ridge-like faults with high-angle tailcracks. Fault motions may be driven by tidal

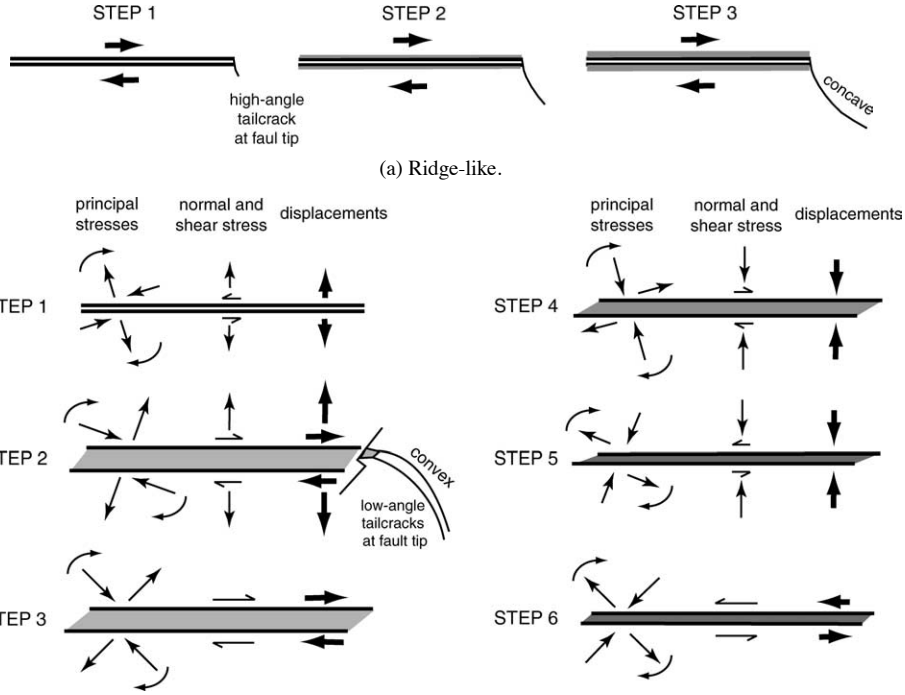

Fig. 10. Conceptual models illustrating the differing sequence of development for ridge-like and band-like faults. (a) Ridge-like faults undergo little to no dilation during slip. In response, tailcracks form with high intersection angles with respect to the fault and are concave towards the direction beyond the fault tip. Ridges may develop on either side of the fault plane due to upwelling of frictionally heated material along the fault walls. (b) Band-like faults develop in a manner analogous to tidal walking theory and can thus be related to the daily rotation of the diurnal tidal stresses. In this example, a southern hemisphere fault is subject to an ongoing clockwise rotation of the diurnal stresses. The fault dilates, facilitating the emplacement of ice from below, then is subject to right-lateral shear that induces low-angle tailcrack growth at the fault tip (shown in step 2 only). The fault then closes, compressing the material within the fault zone as shear stresses become left-lateral and recover some of the accumulated right-lateral offset. Lateral sliding does not occur below a threshold shear stress value, regardless of the shear sense, due to frictional resistance to fault motion. After Step 6, the entire process repeats. Over time, the fault will accumulate increasing right-lateral offsets and the fault zone will widen.

stresses in predominantly compressive stress environments (e.g., Spaun et al., 2003) or may result from some other driving mechanism such as spreading at a nearby smooth band or lateral motions along a different strike-slip fault. With progressive slip accumulation, tailcracks propagate away from the fault, concave towards the direction beyond the fault tip. Frictional heating of the fault walls during slip episodes may cause buoyant upwelling and the construction of ridges (Nimmo and Gaidos, 2002), although this is not necessarily true as the faults may represent reactivated older ridges that formed through some other mechanism. In the model for band-like faults (illustrated for the right-lateral, southern hemisphere case in Fig. 10b), fault motions can be tied directly to the rotating diurnal stress field, which produces variations in resolved normal and shear stresses along the faults, and hence in the slip tendency, during the Europan day. Tidal walking causes a repeating cycle of fault opening and forward slip, producing low-angle tailcracks and emplacement of material into the fault zone from below, then partial closure and deformation of the fault zone material. The partial back-slip predicted by tidal walking may or may not occur depending on available driving stress, which will be site-specific; however, if back-slip does occur, tailcracks that formed during the forward-slip phase would partially close. Regardless of the site-specific stress field, there is likely to be a threshold shear stress below which slip will not occur due to frictional resistance to motion in the fault-closing phase, regardless of the sense of shear (which reverses during a single diurnal cycle).

It is important to keep in mind that the models in Fig. 10 are conceptual. Each individual fault will evolve in a unique manner dependent on local loading conditions. Therefore, these models do not provide explicit driving mechanisms for fault motions, which should clearly be investigated in future studies. For example, Hoppa et al. (1999a) illustrate significant variability in the ratio of shear to normal stress along faults in different locations on Europa during the diurnal cycle. Such variability will cause differences in fault evolutionary history. If dilating faults are subject to internal pressures caused by the emplacement of material from below, then normal stresses will be more tensile than would be produced by diurnal stresses alone, perhaps explaining the seemingly high mode I/mode II ratio of 2 deduced for Agenor. Such complexities are not incorporated into the conceptual models. Nonetheless, the models do provide a mechanically-based interpretation for fault behavior based on observable and quantifiable fault zone characteristics and tailcrack geometries.

The conceptual models can also be used to aid in the interpretation of faults with complex fault zone architectures or seemingly ambiguous tailcrack geometries. For example, ridge-like faults with tailcrack intersection angles that are significantly smaller than 70.5° may have undergone a small amount of dilation during fault motion, assuming the low angle is an accurate measurement and not an artifact of limited image resolution that fails to capture the specifics of the fault/tailcrack intersection point. An exception is where tailcracks that link two fault segments across a stepover zone exhibit a broad-scale low-angle geometry with respect to the faults (e.g., Figs. 5b and 5g), in which case the fault-perturbed stress field within the stepover zone is more complex than for the isolated fault case (Crider and Pollard, 1998; Kattenhorn et al., 2000). Conversely, if a band-like fault exhibits high-angle tailcracks that are more indicative of ridge-like fault behavior (e.g., Fig. 6a), it may be an indication that initial fault slip and tailcrack growth was ridge-like but that the fault zone was subsequently dilated. In the case of the Argadnel Regio example in Fig. 6a, dilation of the fault would be expected as a result of linkage with, and motion along, the differently oriented fault shown in Fig. 5g, located about 90 km to the northwest of Fig. 6a.

The conceptual fault models can also be applied to the most prominent band-like faults on Europa, such as Agenor Linea (Fig. 7) and Astypalaea Linea (Fig. 8a), which have been intensely studied but with interpretations that have not necessarily been compatible. For example, recent work on Agenor Linea has led to less, rather than more, understanding of its origin, nature, and evolution. Agenor Linea was initially described as a compressive band (Schenk and McKinnon, 1989), but was later characterized as a tension crack (Geissler et al., 1998; Greenberg et al., 1998) and then a strike-slip fault with a multi-stage evolutionary history with both extensional and compressive elements (Prockter et al., 2000). Nonetheless, the internal morphology of Agenor Linea, which is up to 30 km wide, suggests broad-scale compressive deformation. Prockter et al. (2000) attribute some of this morphology to strike-slip duplexing, whereas recent work on an Agenor-like feature named Corick Linea, located diametrically opposite to Agenor on the Europan globe, implies that these features represent compressive convergence bands (Greenberg, 2004). Furthermore, the presence of a band-like lineament that branches in a northeasterly sense away from Agenor, in a region where the fault also changes direction abruptly 135 km northwest of the current fault tip, implies a complex evolutionary history for this fault. Nonetheless, the LEFM-based analytical models presented in this study (Fig. 9) clearly demonstrate that the tailcracks at the eastern tip of Agenor, which intersect the fault at $\sim 30°$ and which are convex towards the region beyond the fault tip, necessitated concurrent strike-slip motion and dilation along Agenor. Therefore, at some point in its slip history, Agenor *was* an extensional, right-lateral shear feature. It is possible that the fault subsequently acted as a locus for compressive deformation (e.g., Greenberg, 2004); however, this scenario has yet to be conclusively demonstrated with independent geologic evidence.

In contrast to Agenor, Astypalaea Linea is clearly a dilational strike-slip fault based on its smooth band nature; however the creation of the band material (Fig. 1b) was not due to dilation of the fault walls, as occurred at Agenor and other band-like faults (Figs. 1c, 6, and 7), but was rather a secondary effect due to dilation along the tailcracks as the fault segments underwent lateral displacements. Terrestrial vein-filled tailcracks, or tension gashes, form in this same manner (Rispoli, 1981). The Astypalaea fault segments are thus individually more akin to ridge-like faults, explaining the high tailcrack angles along much of the fault (Fig. 8a), and indicating that the driving stresses responsible for fault motion kept the fault surfaces in contact during slip. Nonetheless, some of the tailcrack angles are low and convex towards the direction beyond the fault tips (such as the 17° tailcrack in Fig. 8a), suggesting that there may also have been a small amount of dilation along some of the fault segments, as confirmed by a rigid-block, structural reconstruction of the fault zone (Fig. 8b). Although there has been some analysis of the development of Astypalaea (Greenberg et al., 1998; Tufts, 1998, PhD thesis; Tufts et al., 1999; Mével and Mercier, 2002), a rigorous structural reconstruction that considers both the relative timing and the slip characteristics of each fault segment is currently lacking. The mechanical indicators for the evolution of Astypalaea presented here should ultimately aid in developing an exact evolutionary history.

5. Conclusions

Strike-slip faults on Europa appear to fall into one of two categories: ridge-like and band-like. The presence of tailcracks along both types of faults can be modeled using linear elastic fracture mechanics theory and justifies the comparison of Europan and terrestrial faults, which are typically modeled in the same manner. Some of the tailcracks on Europa formed at a high angle to the faults that caused them, and indicate pure sliding motion (mode II). These tailcracks curve away from the fault tips in such a manner that they are concave towards the direction beyond the fault tips. Such geometries are almost exclusively characteristic of ridge-like faults. In such examples, any dilational evidence along the faults, such as smooth band material within the fault zone, must have post-dated the strike-slip motion. Many tailcracks form at low angles to strike-slip faults. Analytical models indicate this to be the result of concurrent dilation and strike-slip motion (mixed-mode I–II). Resultant tailcracks curve away from the fault tips in such a manner that they are convex towards the direction beyond the fault tips. Such geometries are exclusively characteristic of band-like faults, indicating a significantly different faulting mechanism to ridge-like faults.

These observations and model results imply that fault dilation is an important component of strike-slip fault motion behavior on Europa (albeit only for band-like faults), as has previously been suggested, but not proven, in conceptual tidal walking models for Europan strike-slip faults. Evidence for fault dilation implies that a significant amount of fault-normal tension is needed during fault slip episodes. Although diurnal tidal stresses may provide sufficient tension, it is also possible that fluid pressures within the fault zone contribute to the driving stress. The conceptual fault models presented here allow for that possibility (for band-like faults) and advocate a distinct difference between the evolution of ridge-like and band-like faults, the underlying cause of which remains to be unraveled.

Acknowledgments

This material is based upon work supported by the National Aeronautics and Space Administration under Grant No. NAG5-11495 issued through the Office of Space Science, and Grant No. NCC5-577 issued through NASA-EPSCoR and the Idaho Space Grant Consortium. Galileo image reprojections were produced using ISIS software distributed by the USGS Astrobiology division. Photomosaics were produced by contributors to the Galileo imaging team. Analytical modeling was based on a Mathematica script developed by Juliet Crider. Thanks to Scott Marshall for assistance with image processing. The author benefited greatly from discussions with Louise Prockter and from rigorous reviews of the original manuscript by Cynthia Phillips and Patricio Figueredo (who also provided fault length measurements for Astypalaea Linea in a south polar reprojection using the GIS Europa database at ASU).

References

Anderson, J.D., Lau, E.L., Sjogren, W.L., Schubert, G., Moore, W.B., 1998. Europa's differentiated internal structure: inferences from four Galileo encounters. Science 276, 1236–1239.

Carr, M.H., Belton, M.J.S., Chapman, C.R., Davies, M.E., Geissler, P., Greenberg, R., McEwen, A.S., Tufts, B.R., Greeley, R., Sullivan, R., Head, J.W., Pappalardo, R.T., Klaasen, K.P., Johnson, T.V., Kaufman, J., Senske, D., Moore, J., Neukum, G., Schubert, G., Burns, J.A., Thomas, P., Veverka, J., 1998. Evidence for a subsurface ocean on Europa. Nature 391, 363–365.

Crider, J.G., Pollard, D.D., 1998. Fault linkage: three-dimensional mechanical interaction between echelon normal faults. J. Geophys. Res. 103, 24373–24391.

Cruikshank, K.M., Zhao, G., Johnson, A.M., 1991. Analysis of minor fractures associated with joints and faulted joints. J. Struct. Geol. 13, 865–886.

Figueredo, P.H., Greeley, R., 2000. Geologic mapping of the northern leading hemisphere of Europa from Galileo solid-state imaging data. J. Geophys. Res. 105, 22629–22646.

Figueredo, P.H., Greeley, R., 2004. Resurfacing history of Europa from pole-to-pole geological mapping. Icarus 167, 287–312.

Geissler, P.E., Greenberg, R., Hoppa, G., McEwen, A., Tufts, R., Phillips, C., Clark, B., Ockert-Bell, M., Helfenstein, P., Burns, J., Veverka, J., Sullivan, R., Greeley, R., Pappalardo, R.T., Head, J.W., Belton, M.J.S., Denk, T., 1998. Evolution of lineaments on Europa: clues from Galileo multispectral imaging observations. Icarus 135, 107–126.

Granier, T., 1985. Origin, damping, and pattern of development of faults in granite. Tectonics 4, 721–737.

Greeley, R., Figueredo, P.H., Williams, D.A., Chuang, F.C., Klemaszewski, J.E., Kadel, S.D., Prockter, L.M., Pappalardo, R.T., Head, J.W., Collins, G.C., Spaun, N.A., Sullivan, R.J., Moore, J.M., Senske, D.A., Tufts, B.R., Johnson, T.V., Belton, M.J.S., Tanaka, K.L., 2000. Geologic mapping of Europa. J. Geophys. Res. 105, 22559–22578.

Greenberg, R., 2004. The evil twin of Agenor: tectonic convergence on Europa. Icarus 167, 313–319.

Greenberg, R., Geissler, P., 2002. Europa's dynamic icy crust. Meteorit. Planet. Sci. 37, 1685–1710.

Greenberg, R., Geissler, P., Hoppa, G., Tufts, B.R., Durda, D.D., Pappalardo, R., Head, J.W., Greeley, R., Sullivan, R., Carr, M.H., 1998. Tectonic processes on Europa: tidal stresses, mechanical response, and visible features. Icarus 135, 64–78.

Helfenstein, P., Parmentier, E.M., 1983. Patterns of fracture and tidal stresses on Europa. Icarus 53, 415–430.

Helfenstein, P., Parmentier, E.M., 1985. Patterns of fracture and tidal stresses due to nonsynchronous rotation: implications for fracturing on Europa. Icarus 61, 175–184.

Hoppa, G., Greenberg, R., Tufts, B.R., Geissler, P., Phillips, C., Milazzo, M., 2000. Distribution of strike-slip faults on Europa. J. Geophys. Res. 105, 22617–22627.

Hoppa, G., Tufts, B.R., Greenberg, R., Geissler, P., 1999a. Strike-slip faults on Europa: global shear patterns driven by tidal stress. Icarus 141, 287–298.

Hoppa, G.V., Tufts, B.R., Greenberg, R., Geissler, P.E., 1999b. Formation of cycloidal features on Europa. Science 285, 1899–1902.

Jaeger, J.C., Cook, N.G.W., 1969. Fundamentals of Rock Mechanics. Methuen, London.

Kattenhorn, S.A., 2002. Nonsynchronous rotation evidence and fracture history in the Bright Plains region, Europa. Icarus 157, 490–506.

Kattenhorn, S.A., 2003. Secondary fracturing of Europa's crust in response to combined slip and dilation along strike-slip faults. In: Proc. Lunar Planet. Sci. Conf. 34th. Lunar and Planetary Institute, Houston. Abstract #1977 [CD-ROM].

Kattenhorn, S.A., 2004. What is (and isn't) wrong with both the tension and shear failure models for the formation of lineae on Europa. In: Workshop on Europa's Icy Shell: Past, Present, and Future, LPI Contribution No. 1195. Lunar and Planetary Institute, Houston, pp. 38–39.

Kattenhorn, S.A., Aydin, A., Pollard, D.D., 2000. Joints at high angles to normal fault-strike: an explanation using 3-D numerical models of fault-perturbed stress fields. J. Struct. Geol. 22, 1–23.

Kim, Y.-S., Andrews, J.R., Sanderson, D.J., 2001. Reactivated strike-slip faults: examples from north Cornwall, UK. Tectonophysics 340, 173–194.

Koenig, E., Aydin, A., 1998. Evidence for large-scale strike-slip faulting on Venus. Geology 26, 551–554.

Lawn, B., 1993. Fracture of Brittle Solids. Cambridge Univ. Press, Cambridge. 378 p.

Marshall, S.T., Kattenhorn, S.A., 2004. Analysis of Europan cycloid morphology and implications for formation mechanisms. In: Workshop on Europa's Icy Shell: Past, Present, and Future, LPI Contribution No. 1195. Lunar and Planetary Institute, Houston, pp. 49–50.

McEwen, A.S., 1986. Tidal reorientation and fracturing of Jupiter's moon, Europa. Nature 321, 49–51.

McKinnon, W.B., 2004. Overview of Europa's icy shell: questions of thickness, composition, rheology, tectonics, and astrobiological potential. In: Workshop on Europa's Icy Shell: Past, Present, and Future, LPI Contribution No. 1195. Lunar and Planetary Institute, Houston, pp. 53–54.

Mével, L., Mercier, E., 2002. Geodynamics on Europa: evidence for a crustal resorption process. In: Proc. Lunar Planet. Sci. Conf. 33rd. Lunar and Planetary Institute, Houston. Abstract #1476 [CD-ROM].

Nemat-Nasser, S., Horii, H., 1982. Compression-induced nonplanar crack extension with application to splitting, exfoliation, and rockburst. J. Geophys. Res. 87, 6805–6821.

Nimmo, F., Gaidos, E., 2002. Strike-slip motion and double ridge formation on Europa. J. Geophys. Res. 107, 1–8.

Pappalardo, R.T., Head, J.W., Sherman, N.D., Greeley, R., Sullivan, R.J., the Galileo Imaging Team, 1998. Classification of Europan ridges and troughs and a possible genetic sequence. In: Proc. Lunar Planet. Sci. Conf. 29th. Lunar and Planetary Institute, Houston. Abstract #1859 [CD-ROM].

Pappalardo, R.T., Belton, M.J.S., Breneman, H.H., Carr, M.H., Chapman, C.R., Collins, G.C., Denk, T., Fagents, S., Geissler, P.E., Giese, B., Greeley, R., Greenberg, J.W., Head, J.W., Helfenstein, P., Hoppa, G., Kadel, S.D., Klaasen, K.P., Klemaszewski, J.E., Magee, K., McEwen, A.S., Moore, J.M., Moore, W.B., Neukum, G., Phillips, C.B., Prockter, L.M., Schubert, G., Senske, D.A., Sullivan, R.J., Tufts, B.R., Turtle, E.P., Wagner, R., Williams, K.K., 1999. Does Europa have a subsurface ocean? Evaluation of the geological evidence. J. Geophys. Res. 104, 24015–24056.

Patterson, G.W., Head, J.W., 2004. Numerical modeling of plate motion: unraveling Europa's tectonic history. In: Workshop on Europa's Icy Shell: Past, Present, and Future, LPI Contribution No. 1195. Lunar and Planetary Institute, Houston, pp. 66–67.

Pollard, D.D., Aydin, A., 1988. Progress in understanding jointing over the past century. Geol. Soc. Am. Bull. 100, 1181–1204.

Pollard, D.D., Segall, P., 1987. Theoretical displacements and stresses near fractures in rock: with applications to faults, joints, veins, dikes, and solution surfaces. In: Atkinson, B.K. (Ed.), Fracture Mechanics of Rock. Academic Press, London, pp. 277–349.

Prockter, L.M., Antman, A.M., Pappalardo, R.T., Head, J.W., Collins, G.C., 1999. Europa: stratigraphy and geological history of the anti-jovian region from Galileo E14 solid-state imaging data. J. Geophys. Res. 104, 16531–16540.

Prockter, L.M., Pappalardo, R.T., Head, J.W., 2000. Strike-slip duplexing on Jupiter's icy moon Europa. J. Geophys. Res. 105, 9483–9488.

Prockter, L.M., Head, J., Pappalardo, R., Sullivan, R., Clifton, A.E., Giese, B., Wagner, R., Neukum, G., 2002. Morphology of Europan bands at high resolution: a mid-ocean ridge-type rift mechanism. J. Geophys. Res. 107, 1–26.

Rispoli, R., 1981. Stress fields about strike-slip faults inferred from stylolites and tension gashes. Tectonophysics 75, T29–T36.

Rist, M.A., Murrell, S.A.F., 1994. Ice triaxial deformation and fracture. J. Glaciol. 40, 305–318.

Sarid, A.R., Greenberg, R., Hoppa, G., Hurford, T.A., Tufts, R., Geissler, P., 2002. Polar wander and surface convergence of Europa's ice shell: evidence from a survey of strike-slip displacement. Icarus 158, 24–41.

Schenk, P., McKinnon, W.B., 1989. Fault offsets and lateral crustal movement on Europa: evidence for a mobile ice shell. Icarus 79, 75–100.

Schulson, E.M., 2002. On the origin of a wedge crack within the icy crust of Europa. J. Geophys. Res. 107, 1–9.

Spaun, N.A., Pappalardo, R.T., Head, J.W., 2003. Evidence for shear failure in forming near-equatorial lineae on Europa. J. Geophys. Res. 108 (E6), 5060. 14-1–14-21.

Tufts, B.R., Greenberg, R., Hoppa, G., Geissler, P., 1999. Astypalaea Linea: a large-scale strike-slip fault on Europa. Icarus 141, 53–64.

Tufts, B.R., Greenberg, R., Hoppa, G., Geissler, P., 2000. Dilation of the Europan lithosphere. In: Proc. Lunar Planet. Sci. Conf. 31st. Lunar and Planetary Institute, Houston. Abstract #1773 [CD-ROM].

Willemse, E.J.M., Peacock, D.C.P., Aydin, A., 1998. Nucleation and growth of strike-slip faults in limestone. J. Struct. Geol. 19, 1461–1477.